

Scalable Bayesian shrinkage and uncertainty quantification for high-dimensional regression

Bala Rajaratnam*

Department of Statistics, University of California, Davis

Doug Sparks*

Department of Statistics, Stanford University

Kshitij Khare[†]

Department of Statistics, University of Florida

Liyuan Zhang

Department of Statistics, University of Florida

April 21, 2017

Abstract

Bayesian shrinkage methods have generated a lot of recent interest as tools for high-dimensional regression and model selection. These methods naturally facilitate tractable uncertainty quantification and incorporation of prior information. This benefit has led to extensive use of the Bayesian shrinkage methods across diverse applications. A common feature of these models, including the Bayesian lasso, global-local shrinkage priors, spike-and-slab priors is that the corresponding priors on the regression coefficients can be expressed as scale mixture of normals. While the three-step Gibbs sampler used to sample from the often intractable associated posterior density has been shown to be geometrically ergodic for several of these models (Khare and Hobert, 2013; Pal and Khare, 2014), it has been demonstrated recently that convergence of this sampler can still be quite slow in modern high-dimensional settings despite this apparent theoretical safeguard. In order to address this challenge, we propose a new method to draw from the same posterior via a tractable two-step blocked Gibbs sampler. We demonstrate that our proposed two-step blocked sampler exhibits vastly superior convergence behavior compared to the original three-step sampler in high-dimensional regimes on both real and simulated data. We also provide a detailed theoretical underpinning to the

*Authors supported in part by the US National Science Foundation under grants DMS-CMG-1025465, AGS-1003823, DMS-1106642, and DMS-CAREER-1352656, and by the US Air Force Office of Scientific Research grant award FA9550-13-1-0043.

[†]Author supported in part by NSF grant DMS-15-11945.

new method in the context of the Bayesian lasso. First, we prove that the proposed two-step sampler is geometrically ergodic, and derive explicit upper bounds for the (geometric) rate of convergence. Furthermore, we demonstrate theoretically that while the original Bayesian lasso chain is not Hilbert–Schmidt, the proposed chain is trace class (and hence Hilbert–Schmidt). The trace class property has useful theoretical and practical implications. It implies that the corresponding Markov operator is compact, and its (countably many) eigenvalues are summable. It also facilitates a rigorous comparison of the two-step blocked chain with “sandwich” algorithms which aim to improve performance of the two-step chain by inserting an inexpensive extra step.

Keywords: Bayesian shrinkage; Gibbs sampler; Hilbert–Schmidt operator; Markov chain; Scale mixture of normals.

1 Introduction

In modern statistics, high-dimensional datasets, where the number of covariates/features is more than the number of samples, are very common. Penalized likelihood methods such as the lasso (Tibshirani, 1996) and its variants simultaneously inducing shrinkage and sparsity in the estimation of regression coefficients. These goals are especially desirable when the number of coefficients to be estimated is greater than the sample size. One drawback of these penalized method is that it is not immediately obvious how to provide meaningful uncertainty quantification for the coefficient estimates. An alternative solution is to pursue a Bayesian approach by using shrinkage priors - priors that shrink the coefficients towards zero, by either having a discrete point mass component at zero (e.g., spike and slab priors George and McCulloch (1993)) or a continuous density with a peak at zero. The uncertainty of the resulting estimates can be quantified in a natural way through the usual Bayesian framework (e.g., credible intervals).

In fact, one can interpret the lasso objective function (or some monotone transformation thereof) as the posterior under a certain Bayesian model with an independent Laplace prior on the coefficients, as was noted immediately by Tibshirani, and developed further by Park and Casella Park and Casella (2008) into the Bayesian lasso approach. Following the Bayesian lasso, a rich and interesting class of “continuous global-local shrinkage priors” has been developed in recent years. (see, for example, Armagan et al., 2013b; Carvalho et al., 2010; Griffin and Brown, 2010; and the references therein). The priors are typically scale mixtures of normals, and have a peak at zero to promote shrinkage.

However, for most of these methods, the resulting intractable posterior is not adequately tractable to permit the closed-form evaluation of integrals. To address this problem, the respective authors have typically proposed a three-block Gibbs sampler based on a hierarchical formulation of the prior structure. This structure, which is essentially a type of data

augmentation, leads to a tractable three- step Gibbs sampler (one step for β , σ^2 and the augmented parameter block each) that can be used to draw from the desired posterior. These posterior samples can then be used to construct credible intervals or other quantities of interest.

Bayesian shrinkage methods (including the Bayesian lasso) have been extensively used in applications as diverse as genetics, finance, ecology, image processing, neuroscience, and clinical trials, receiving over 1,000 citations in total (see, for example, [Yi and Xu, 2008](#); [de los Campos et al., 2009](#); [DeMiguel et al., 2009](#); [Jacquemin and Doll, 2014](#); [Xing et al., 2012](#); [Mishchenko and Paninski, 2012](#); [Gu et al., 2013](#); [Pong-Wong, 2014](#); [Pong-Wong and Woolliams, 2014](#)) example). Nevertheless, the three-step Gibbs sampling schemes needed to implement these methods in practice can require considerable computational resources. Such computational concerns have primarily limited the application of these approaches to problems of only moderately high dimension (e.g., in the tens or hundreds of variables). This is often a serious shortcoming since for many modern applications, the number of variables p is in the thousands if not more. Thus, methods to analyze or improve the efficiency of the Bayesian lasso algorithm, in terms of either computational complexity or convergence properties, are an important topic of research for modern high-dimensional settings.

[Khare and Hobert \(2013\)](#) proved that the three-step Gibbs sampler of [Park and Casella](#) (which works for arbitrary n and p) is geometrically ergodic for arbitrary values of n and p and they provide a quantitative upper bound for the geometric rate constant. Geometric ergodicity of the three-step samplers for the Normal-Gamma and Dirichlet-Laplace shrinkage models ([Griffin and Brown \(2010\)](#) and [Bhattacharya et al. \(2015\)](#), respectively) was established in [Pal and Khare \(2014\)](#). However, it has been demonstrated that the geometric rate constant does indeed tend to 1 if $p/n \rightarrow \infty$ ([Rajaratnam and Sparks, 2015](#)). Thus, despite the apparent theoretical safeguard of geometric ergodicity, these three-step Gibbs samplers can take arbitrarily long to converge (to within a given total variation distance of the true posterior) if p/n is large enough. This fact is problematic since the so-called “small n , large p ” setting is precisely where the use of the lasso and other regularized regression methods is most beneficial and hence most commonly espoused.

Since the convergence properties of the original three-step Bayesian lasso Gibbs sampler deteriorate in high-dimensional regimes, it may be asked whether there exist alternative schemes for sampling from the same posterior that maintain a reasonably fast (i.e., small) geometric convergence rate when p is large compared to n . Two commonly employed approaches to constructing such alternative MCMC schemes within the Gibbs sampling context are known as *collapsing* and *blocking*. In a collapsed Gibbs sampler, one or more parameters are integrated out of the joint posterior, and a Gibbs sampler is constructed on

the posterior of the remaining parameters. Although a collapsed Gibbs sampler converges at least as fast as its uncollapsed counterpart (Liu et al., 1994), the resulting distributions may not be adequately tractable to permit the implementation of such a scheme in practice. In a blocked Gibbs sampler (also called a grouped Gibbs sampler), multiple parameters are combined and sampled simultaneously in a single step of the cycle that forms each iteration. It is generally understood that blocking usually improves the convergence rate with a careful choice of which parameters to group into the same step (Liu et al., 1994).

In this paper, we propose a two-step/two-block Gibbs sampler in which the regression coefficients β and the residual variance σ^2 are drawn in the same step of the Gibbs sampling cycle. This method turns out to be just as tractable as the original three-step/three-block Gibbs samplers. Indeed, the distributional forms of our proposed sampler coincide with the original chains, differing only in the shape and scale of the inverse gamma distribution from which σ^2 is drawn. Also, unlike the original three-step/three-block Gibbs chain, the two-step/two-block chain is reversible. We demonstrate empirically that in regimes where p is much larger than n , the convergence rate of the proposed two-block Gibbs samplers are vastly superior to those of the original three-block schemes.

Next, we undertake a rigorous investigation into the theoretical properties of the proposed two-block chain in the context of the Bayesian lasso. We first establish geometric ergodicity for the blocked chain, and obtain an explicit upper bound for the rate of convergence. Geometric ergodicity (along with other mild regularity conditions) implies the existence of a Markov chain CLT, which allows users to provide standard errors for Markov chain based estimates of posterior quantities.

We also prove that the (non-self-adjoint) Markov operator associated with the original Gibbs sampling Markov chain is not Hilbert–Schmidt (eigenvalues of the absolute value of this operator are not square-summable) for all n and p . On the other hand, we prove that the (positive, self-adjoint) Markov operator associated with the proposed blocked chain is trace-class (eigenvalues are in fact summable, and hence square-summable). Note that all the aforementioned eigenvalues are less than 1 in absolute value. These results indicate that the proposed Markov chain is more efficient than the original three-step Bayesian lasso chain. The blocked Markov chain can also be regarded as a Data Augmentation algorithm. Sandwich algorithms, which aim to improve the performance of DA algorithms by inserting an inexpensive extra step between the two steps of the DA algorithm, have gained a lot of attention in recent years (see Liu and Wu (1999); Meng and van Dyk (1999); Hobert and Marchev (2008); Khare and Hobert (2011) and the references therein). The trace class property for the blocked chain, along with results from Khare and Hobert (2011), guarantees that a large variety of sandwich Markov chains are themselves trace class, and their eigenvalues

are dominated by the corresponding eigenvalues of the blocked chain (with at least one strict domination). Thus, our trace class result provides theoretical support for the use of sandwich Markov chains to further improve speed and efficiency for sampling from the desired Bayesian lasso posterior distribution.

It is well-understood (see for example [Jones and Hobert \(2001\)](#)) that proving geometric ergodicity and trace class/Hilbert Schmidt properties for practical Markov chains such as these can be rather tricky and *a matter of art*, where each Markov chain requires a genuinely unique analysis based on its specific structure. Hence, a theoretical study of the two-step and three-step Markov chains (similar to the study undertaken in this paper for the Bayesian lasso) is a big and challenging undertaking, and is the task of ongoing and future research.

The remainder of the paper is organized as follows. In [Section 2](#), we revisit the original three-step chain. We propose the two-step chain in [Section 3](#). [Section 4](#) provides a numerical comparison of the original and the proposed versions for both Bayesian lasso and the spike and slab priors (as representatives from the classes of continuous and discrete shrinkage priors) on simulated data, while [Section 5](#) does the same for real data. We then focus on the theoretical properties of the original and proposed methods in the context of the Bayesian lasso model, and undertake a rigorous investigation in [Section 6](#).

2 Bayesian shrinkage for regression

Consider the model

$$\mathbf{Y} \mid \boldsymbol{\beta}, \sigma^2 \sim N_n(\mu \mathbf{1}_n + \mathbf{X}\boldsymbol{\beta}, \sigma^2 \mathbf{I}_n), \quad (1)$$

where $\mathbf{Y} \in \mathbb{R}^n$ is a response vector, \mathbf{X} is a known $n \times p$ design matrix of standardized covariates, $\boldsymbol{\beta} \in \mathbb{R}^p$ is an unknown vector of regression coefficients, $\sigma^2 > 0$ is an unknown residual variance, and $\mu \in \mathbb{R}$ is an unknown intercept. As mentioned previously, in modern applications, often the number of covariates p is much larger than the sample size n . To obtain meaningful estimates and identify significant covariates in this challenging situation, a common and popular approach is to shrink the regression coefficients towards zero. In the Bayesian paradigm, this can be achieved by using spike and slab priors, which are mixtures of a normal density with a spike at zero (low variance) and another normal density which is flat near zero (high variance), see [Mitchell and Beauchamp \(1988\)](#); [George and McCulloch \(1993\)](#). A popular and more computationally efficient alternative is to use “continuous” shrinkage prior densities that have a peak at zero, and tails approaching zero at an appropriate rate, see [Park and Casella \(2008\)](#); [Carvalho et al. \(2010\)](#); [Polson and Scott \(2010\)](#); [Kyung et al. \(2010\)](#);

Griffin and Brown (2010); Armagan et al. (2013a); Polson et al. (2013) and the references therein.

A common thread that runs through all the above shrinkage priors for high-dimensional regression is that they all can be expressed as scale mixtures of normal densities. In particular, the prior density for these models can be specified as

$$\boldsymbol{\beta} \mid \sigma^2, \boldsymbol{\tau} \sim N_p(\mathbf{0}_p, \sigma^2 \mathbf{D}_{\boldsymbol{\tau}}), \quad \boldsymbol{\tau} \sim \pi(\boldsymbol{\tau}), \quad (2)$$

where $\pi(\boldsymbol{\tau})$ is a prior on $\boldsymbol{\tau} = (\tau_1, \dots, \tau_p)$. Suppose further that the prior on σ^2 and μ is once again the improper prior $\pi(\sigma^2, \mu) = 1/\sigma^2$ and that this prior is independent of the prior on $\boldsymbol{\tau}$. After combining this prior structure with the basic regression model in (1) and integrating out μ , the remaining full conditional distributions are

$$\begin{aligned} \boldsymbol{\tau} \mid \boldsymbol{\beta}, \sigma^2, \mathbf{Y} &\sim \pi(\boldsymbol{\tau} \mid \boldsymbol{\beta}, \sigma^2, \mathbf{Y}), \\ \sigma^2 \mid \boldsymbol{\beta}, \boldsymbol{\tau}, \mathbf{Y} &\sim \text{InverseGamma}\left[(n+p-1)/2, \|\tilde{\mathbf{Y}} - \mathbf{X}\boldsymbol{\beta}\|_2^2/2 + \boldsymbol{\beta}^T \mathbf{D}_{\boldsymbol{\tau}}^{-1} \boldsymbol{\beta}/2\right], \\ \boldsymbol{\beta} \mid \sigma^2, \boldsymbol{\tau}, \mathbf{Y} &\sim N_p\left(\mathbf{A}_{\boldsymbol{\tau}}^{-1} \mathbf{X}^T \tilde{\mathbf{Y}}, \sigma^2 \mathbf{A}_{\boldsymbol{\tau}}^{-1}\right), \end{aligned} \quad (3)$$

where $\mathbf{A}_{\boldsymbol{\tau}} = \mathbf{X}^T \mathbf{X} + \mathbf{D}_{\boldsymbol{\tau}}^{-1}$ and $\mathbf{D}_{\boldsymbol{\tau}} = \text{Diag}(\tau_1, \tau_2, \dots, \tau_p)$. If it is feasible to draw from $\pi(\boldsymbol{\tau} \mid \boldsymbol{\beta}, \sigma^2, \mathbf{Y})$, then the three conditionals above may be used to construct a useful three-step Gibbs sampler to draw from the joint posterior $\pi(\boldsymbol{\beta}, \sigma^2 \mid \mathbf{Y})$. The one-step transition density \hat{k} with respect to Lebesgue measure on $\mathbb{R}^p \times \mathbb{R}_+$ given by

$$\hat{k}[(\boldsymbol{\beta}_0, \sigma_0^2), (\boldsymbol{\beta}_1, \sigma_1^2)] = \int_{\mathbb{R}_+^p} \pi(\sigma_1^2 \mid \boldsymbol{\beta}_1, \boldsymbol{\tau}, \mathbf{Y}) \pi(\boldsymbol{\beta}_1 \mid \boldsymbol{\tau}, \sigma_0^2, \mathbf{Y}) \pi(\boldsymbol{\tau} \mid \boldsymbol{\beta}_0, \sigma_0^2, \mathbf{Y}) d\boldsymbol{\tau}. \quad (4)$$

Many commonly used Bayesian methods for high-dimensional regression can be characterized in the form of the priors in (2) and the Gibbs sampler in (3). We now present a few such examples.

2.1 Spike-and-Slab Prior

Now suppose instead that the τ_j are assigned independent discrete priors that each assign probability w_j to the point $\kappa_j \zeta_j$ and probability $1 - w_j$ to the point ζ_j , where $\zeta_j > 0$ is small, $\kappa_j > 0$ is large, and $0 < w_j < 1$. This formulation is a slight modification of the prior proposed by George and McCulloch (1993) to approximate the spike-and-slab prior of Mitchell and Beauchamp (1988). Then the conditional posterior distribution of $\boldsymbol{\tau} \mid \boldsymbol{\beta}, \sigma^2, \mathbf{Y}$ is a product of independent discrete distributions that each assign probability \tilde{w}_j to the

point $\kappa_j \zeta_j$ and probability $1 - \tilde{w}_j$ to the point ζ_j , where

$$\tilde{w}_j = \left\{ 1 + \frac{(1 - w_j)\sqrt{\kappa_j}}{w_j} \exp \left[-\frac{\beta_j^2}{2\sigma^2} \left(\frac{\kappa_j - 1}{\kappa_j \zeta_j} \right) \right] \right\}^{-1}$$

by straightforward modification of the results of [George and McCulloch \(1993\)](#).

2.2 The Bayesian lasso

Suppose that the τ_j 's are assigned independent $Exponential(\lambda^2/2)$ priors. It follows that the marginal prior of $\boldsymbol{\beta}$ (given σ^2) assigns independent Laplace densities to each component. In fact, the posterior mode in this setting is precisely the lasso estimate of [Tibshirani \(1996\)](#). Hence, Park and Casella [Park and Casella \(2008\)](#) refer to this approach as the Bayesian lasso. In this setting, the conditional posterior distribution of $\boldsymbol{\tau} \mid \boldsymbol{\beta}, \sigma^2, \mathbf{Y}$ assigns independent inverse Gaussian distributions to each $1/\tau_j$, and hence is easy to sample from.

Following the three-step Gibbs sampler of [Park and Casella](#), two useful alternative Gibbs samplers for sampling from the Bayesian lasso posterior were proposed by [Hans \(2009\)](#). However, both samplers, namely the standard and the orthogonal sampler, require a sample size n at least as large as the number of variables p , since they require the design matrix to have full column rank. The standard sampler can perform poorly when the predictors are highly correlated, while the orthogonal sampler becomes very computationally expensive as p grows (recall that p still must be less than n). The $n > p$ assumption can thus be a serious limitation, as it precisely excludes the high-dimensional settings targeted by the Bayesian lasso.

2.3 Global-local continuous shrinkage priors

Suppose we assume that $\tau_j = \eta \lambda_j$ for $j = 1, 2, \dots, p$. Here, η controls global shrinkage towards the origin while the local scale parameters λ_j allow component wise deviations in shrinkage. Hence, these priors are called as global-local shrinkage priors. A variety of global-local shrinkage priors have been proposed in the Bayesian literature, see [Polson and Scott \(2010\)](#); [Bhattacharya et al. \(2015\)](#) for an exhaustive list. For almost all of these models, sampling from the posterior distribution is performed by using a three-block Gibbs sampler, with $\boldsymbol{\beta}$ and σ^2 being two of the blocks, and all the shrinkage parameters (local and global) being the third block. As an example, we consider the Dirichlet-Laplace shrinkage prior from [Bhattacharya et al. \(2015\)](#). The regression version of this model was considered in [Pal and](#)

Khare (2014), and is provided as follows.

$$\begin{aligned}
\mathbf{y} \mid \boldsymbol{\beta}, \sigma^2 &\sim N(X\boldsymbol{\beta}, \sigma^2 I_n) \\
\boldsymbol{\beta} \mid \sigma^2, \boldsymbol{\psi}, \boldsymbol{\phi}, \theta &\sim N(0, \sigma^2 D_{\boldsymbol{\tau}}) \text{ where } \tau_j = \psi_j \phi_j^2 \theta^2 \\
\sigma^2 &\sim \text{Inverse-Gamma}(\alpha, \xi) \quad \alpha, \xi > 0 \text{ fixed} \\
\psi_1, \psi_2, \dots, \psi_p &\stackrel{i.i.d.}{\sim} \text{Exp}\left(\frac{1}{2}\right) \\
(\phi_1, \phi_2, \dots, \phi_p) &\sim \text{Dir}(a, a, \dots, a), \theta \sim \text{Gamma}\left(pa, \frac{1}{2}\right). \tag{5}
\end{aligned}$$

Here $\boldsymbol{\eta} = (\boldsymbol{\psi}, \boldsymbol{\phi}, \theta)$ denotes the collection of all shrinkage parameters, and a is a known positive constant. It can be seen that the full conditional distributions of $\boldsymbol{\beta}$ and σ^2 are exactly the same as in (3). Based on results in Bhattacharya et al. (2015), it is shown in Pal and Khare (2014) that samples from the full conditional distribution of $\boldsymbol{\eta}$ can be generated by making draws from a bunch of appropriate Generalized Inverse Gaussian densities.

2.4 Student's t Prior

First, suppose that the τ_j are assigned independent inverse-gamma priors with shape parameter $\nu_j/2$ and scale parameter $\eta_j/2$. This structure corresponds (by integrating out $\boldsymbol{\tau}$) to specification of the prior on $\boldsymbol{\beta} \mid \sigma^2$ as a product of independent scaled Student's t priors, where the prior on each $\beta_j \mid \sigma^2$ has ν_j degrees of freedom and scale parameter $(\eta_j \sigma^2)^{1/2}$. Such Student's t priors are a popular choice when a mildly informative prior is desired (see, e.g., Gelman et al., 2013). In this case, the conditional posterior distribution of $\boldsymbol{\tau} \mid \boldsymbol{\beta}, \sigma^2, \mathbf{Y}$ is a product of independent inverse-gamma distributions, where the distribution of each $\tau_j \mid \boldsymbol{\beta}, \sigma^2, \mathbf{Y}$ has shape parameter $(\nu_j + 1)/2$ and scale parameter $(\eta_j + \beta_j^2/\sigma^2)/2$.

2.5 Bayesian Elastic Net

As a final example, suppose instead that the τ_j are assigned independent continuous priors, each with density

$$\pi(\tau_j) = \frac{\lambda_1}{2(1 - \lambda_2 \tau_j)^2} \exp\left[-\frac{\lambda_1 \tau_j}{2(1 - \lambda_2 \tau_j)}\right]$$

with respect to Lebesgue measure on the interval $(0, \lambda_2^{-1})$, where $\lambda_1, \lambda_2 > 0$. This structure corresponds (by integrating out $\boldsymbol{\tau}$) to specification of the prior on $\boldsymbol{\beta} \mid \sigma^2$ as a product of independent priors, where the prior on each $\beta_j \mid \sigma^2$ has density with respect to Lebesgue

measure that is proportional to

$$\pi(\beta_j | \sigma^2) \propto \exp\left(-\sqrt{\frac{\lambda_1}{\sigma^2}} |\beta_j| - \frac{\lambda_2}{2\sigma^2} \beta_j^2\right).$$

Then the conditional posterior distribution of $\boldsymbol{\tau} | \boldsymbol{\beta}, \sigma^2, \mathbf{Y}$ is

$$\left(\frac{1}{\tau_j} - \lambda_2\right) \Big| \boldsymbol{\beta}, \sigma^2, \mathbf{Y} \sim \text{ind InverseGaussian}\left(\sqrt{\frac{\lambda_1 \sigma^2}{\beta_j^2}}, \lambda_1\right).$$

This prior structure and corresponding Gibbs sampler are known as the Bayesian elastic net (Li and Lin, 2010; Kyung et al., 2010).

3 The fast Bayesian shrinkage algorithm

While the three-step Gibbs sampler (with transition density \hat{k}) provides a useful and straightforward way to sample from the posterior density, its slow convergence in high-dimensional settings with $p \gg n$ is discussed by Rajaratnam and Sparks (2015). In particular, it is demonstrated that the slow convergence problem in these settings arises due to the high a posteriori dependence between $\boldsymbol{\beta}$ and σ^2 . It was argued by Liu et al. (1994) that the convergence rate of Gibbs samplers can often be improved by grouping highly dependent parameters together into a single block of a blocked Gibbs sampler. Of course, if the conditional densities for the blocked Gibbs sampler are not easy to sample from, then any possible gain from blocking is likely to be overshadowed by the extra effort in sampling from such densities.

In an effort to address the slow convergence of the three-step Gibbs sampler in high-dimensional settings, we prove the following lemma. Its proof may be found in the Supplementary Material.

Lemma 1. *For the Bayesian model in (2), $\sigma^2 | \boldsymbol{\tau}, \mathbf{Y}$ has the inverse gamma distribution with shape parameter $(n - 1)/2$ and scale parameter $\tilde{\mathbf{Y}}^\top (\mathbf{I}_n - \mathbf{X} \mathbf{A}_\tau^{-1} \mathbf{X}^\top) \tilde{\mathbf{Y}}/2$.*

This lemma facilitates the construction of a novel blocked two-step Gibbs sampler which can be used to generate samples from the joint posterior density of $(\boldsymbol{\beta}, \sigma^2)$, and which is as tractable as the original three-step Gibbs sampler. This blocked Gibbs sampler alternates between drawing $(\boldsymbol{\beta}, \sigma^2) | \boldsymbol{\tau}$ and $\boldsymbol{\tau} | (\boldsymbol{\beta}, \sigma^2)$. In particular, $(\boldsymbol{\beta}, \sigma^2) | \boldsymbol{\tau}$ may be drawn by first drawing $\sigma^2 | \boldsymbol{\tau}$ and then drawing $\boldsymbol{\beta} | \sigma^2, \boldsymbol{\tau}$. In other words, the blocked Gibbs sampler may be constructed by replacing the draw of $\sigma^2 | \boldsymbol{\beta}, \boldsymbol{\tau}, \mathbf{Y}$ in (3) with a draw of $\sigma^2 | \boldsymbol{\tau}$ as given by Lemma 1. In particular, the blocked Gibbs sampler cycles through drawing from the

distributions

$$\begin{aligned} \boldsymbol{\tau} \mid \boldsymbol{\beta}, \sigma^2, \mathbf{Y} &\sim \pi(\boldsymbol{\tau} \mid \boldsymbol{\beta}, \sigma^2, \mathbf{Y}) \\ (\boldsymbol{\beta}, \sigma^2) \mid \boldsymbol{\tau}, \mathbf{Y} &\sim \begin{cases} \sigma^2 \mid \boldsymbol{\tau}, \mathbf{Y} \sim \text{InverseGamma}\left[(n-1)/2, \tilde{\mathbf{Y}}^T(\mathbf{I}_n - \mathbf{X}\mathbf{A}_{\boldsymbol{\tau}}^{-1}\mathbf{X}^T)\tilde{\mathbf{Y}}/2\right], \\ \boldsymbol{\beta} \mid \sigma^2, \boldsymbol{\tau}, \mathbf{Y} \sim N_p\left(\mathbf{A}_{\boldsymbol{\tau}}^{-1}\mathbf{X}^T\tilde{\mathbf{Y}}, \sigma^2\mathbf{A}_{\boldsymbol{\tau}}^{-1}\right), \end{cases} \end{aligned} \quad (6)$$

and has one-step transition density k with respect to Lebesgue measure on $\mathbb{R}^p \times \mathbb{R}_+$ given by

$$k[(\boldsymbol{\beta}_0, \sigma_0^2), (\boldsymbol{\beta}_1, \sigma_1^2)] = \int_{\mathbb{R}_+^p} \pi(\boldsymbol{\tau} \mid \boldsymbol{\beta}_0, \sigma_0^2, \mathbf{Y}) \pi(\sigma_1^2 \mid \boldsymbol{\tau}, \mathbf{Y}) \pi(\boldsymbol{\beta}_1 \mid \sigma_1^2, \boldsymbol{\tau}, \mathbf{Y}) d\boldsymbol{\tau}. \quad (7)$$

Note that the blocked Gibbs sampler is just as tractable as the original sampler since the only the parameters of the inverse gamma distribution are modified. In particular, although the blocked Gibbs sampler requires inversion of the matrix $\mathbf{A}_{\boldsymbol{\tau}}$ to draw σ^2 , this inversion must be carried out anyway to draw $\boldsymbol{\beta}$, so no real increase in computation is required.

Note that our Markov chains move on the $(\boldsymbol{\beta}, \sigma^2)$ space as these are the parameters of interest. In other words, we integrate out the augmented parameter $\boldsymbol{\tau}$ when we compute our transition densities \hat{k} and k in (4) and (7) respectively. If we consider the “lifted versions” of our chains where we move on the $(\boldsymbol{\beta}, \sigma^2, \boldsymbol{\tau})$ space (do not integrate out $\boldsymbol{\tau}$ for the transition densities), then the results in Liu et al. (1994) imply that the Markov operator corresponding to the two-step chain has a smaller operator norm as compared to the three-step chain. However, no comparisons of the spectral radius, which dictates the rate of convergence of the non-reversible lifted chains, is available. Furthermore, no theoretical comparison of the actual Markov chains (with transition densities \hat{k} and k) is available. Hence, in subsequent sections, we undertake a numerical comparison (on both simulated and real data) as well as a theoretical comparison of the proposed two-step sampler and the original three-step sampler.

Remark. Note that in the case of many global-local shrinkage priors such as in Section 2.3, $\boldsymbol{\tau}$ is a function of the global and local shrinkage parameters. Hence, to sample from $\boldsymbol{\tau}$, one needs to sample from the conditional distribution of the collection of shrinkage parameters (denoted by $\boldsymbol{\eta}$ in Section 2.3) given $\boldsymbol{\beta}$ and σ^2 . However, the distribution of $(\boldsymbol{\beta}, \sigma^2)$ depends on $\boldsymbol{\eta}$ only through $\boldsymbol{\tau}$, and samples from the joint density of $(\boldsymbol{\beta}, \sigma^2)$ given $\boldsymbol{\eta}$ can be generated exactly as described in (6).

Remark. We use the term *blocked* rather than *grouped* to avoid confusion with existing methods such as the *group Bayesian lasso* (Kyung et al., 2010), in which the notion of grouping is unrelated to the concept considered here. Note also that the original three-step sampler could already be considered a blocked Gibbs sampler since the β_j and τ_j are not

drawn individually. Thus, our use of the term *blocked* in describing the proposed two-step sampler should be understood as meaning that the Gibbs sampling cycle is divided into fewer blocks than in the original Gibbs sampler.

4 Numerical Comparison

Note that as illustrated in Section 2 our approach is applicable to a wide variety of Bayesian high-dimensional regression methods. In this section, we will undertake a numerical comparison between the convergence rates and efficiency of the original and proposed chains for two such methods. One is the spike-and-slab approach from 2.1 (representing methods with point mass or discrete shrinkage priors), and the second one is Bayesian lasso approach from Section 2.2 (representing continuous shrinkage priors). As a proxy for the actual rate of convergence of the chain, we consider the autocorrelation in the marginal σ_k^2 chain. Note that this autocorrelation is exactly equal to the geometric convergence rate in the simplified case of standard Bayesian regression (Rajaratnam and Sparks, 2015) and is a lower bound for the true geometric convergence rate in general (Liu et al., 1994).

4.1 Numerical comparison for Bayesian lasso

Figure 1 plots the autocorrelation for the original three-step and proposed two-step Bayesian lasso Gibbs samplers versus p for various values of n . (Similar plots under varying sparsity and multicollinearity may be found in the Supplementary Material). The left side of Figure 2 plots the same autocorrelation versus $\log(p/n)$ for a wider variety of values of n and p . It is apparent that this autocorrelation for the proposed two-step Bayesian lasso is bounded away from 1 for all n and p . The center and right side of Figure 2 show dimensional autocorrelation function (DACF) surface plots (see Rajaratnam and Sparks, 2015) for the original (left) and (right) Bayesian lasso Gibbs samplers. (See the Supplementary Material for details of the generation of the various numerical quantities that were used in the execution of these chains). It is clear that the autocorrelation tends to 1 as $p/n \rightarrow \infty$ for the original Bayesian lasso but remains bounded away from 1 for the proposed two-step Bayesian lasso.

4.2 Numerical comparison for spike and slab

We also applied both spike-and-slab Gibbs samplers to simulated data that was constructed in a manner identical to the simulated data for the Bayesian lasso in Figure 1. The resulting autocorrelations of the σ_k^2 chains are shown in Figure 3. As with the Bayesian lasso, it is clear that the two-step blocked version of the spike-and-slab sampler exhibits dramatically

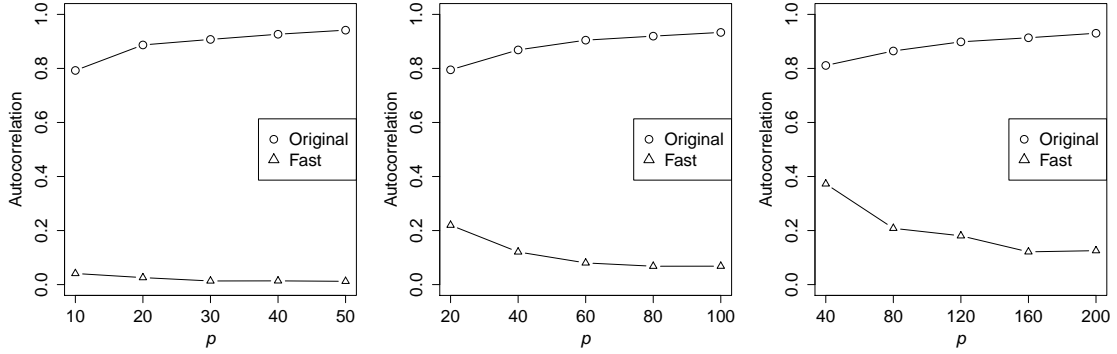


Figure 1: Autocorrelation of σ_k^2 versus p for the original three-step and proposed two-step Bayesian lasso Gibbs samplers with $n = 5$ (left), $n = 10$ (center), and $n = 20$ (right). See the Supplementary Material for details of the generation of the numerical quantities used in the execution of these chains.

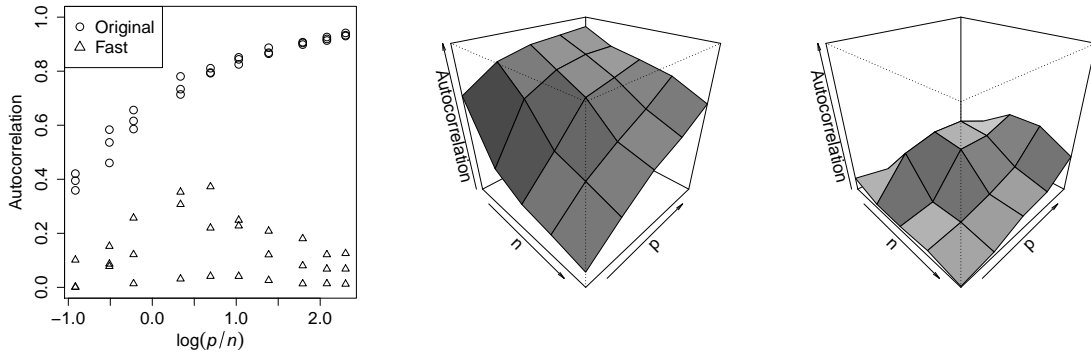


Figure 2: Autocorrelation of σ_k^2 versus $\log(p/n)$ for the original three-step and proposed two-step Bayesian lasso Gibbs samplers with various values of n and p (left). Dimensional autocorrelation function (DACF) surface plots for the σ_k^2 chain relative to n and p for the original (center) and two-step (right) Bayesian lasso Gibbs samplers. See the Supplementary Material for details of the generation of the numerical quantities used in the execution of these chains.

improved convergence behavior in terms of n and p as compared to the original three-step sampler.

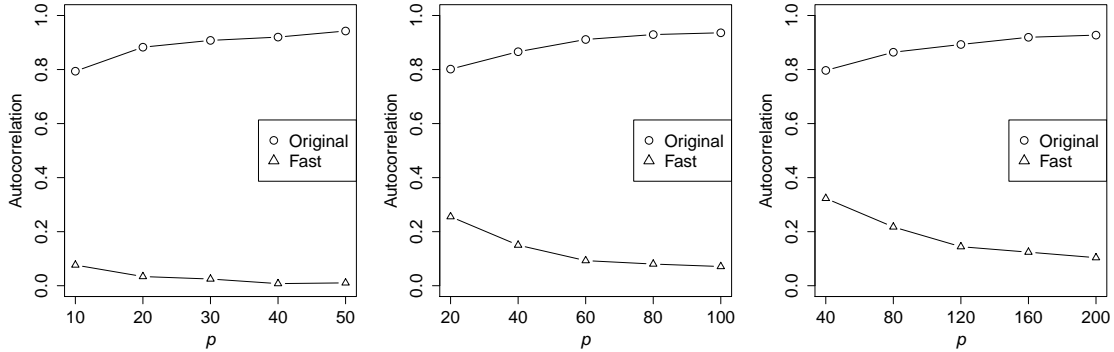


Figure 3: Autocorrelation of σ_k^2 versus p for the original two-step and proposed three-step spike-and-slab Gibbs samplers with $n = 5$ (left), $n = 10$ (center), and $n = 20$ (right). See the Supplementary Material for details of the generation of the numerical quantities used in the execution of these chains.

5 Applications to Real Data

We now illustrate the benefits of the proposed two-step approach through its application to three readily available regression data sets.

5.1 Gene Expression Data

5.1.1 Results for Bayesian lasso

We first evaluate the performance of the original and proposed chains using the Bayesian lasso model through their application to the gene expression data of [Scheetz et al. \(2006\)](#), which is publicly available as the data set `eyedata` in the R package `flare` ([Li et al., 2014](#)). This data set includes $n = 120$ observations of a response variable and $p = 200$ covariates. The columns of \mathbf{X} were standardized to have mean zero and squared Euclidean norm n . The regularization parameter was taken to be $\lambda = 0.2185$ so that the number of nonzero coefficients in the lasso estimate is $\min\{n, p\}/2 = 60$. Both the original three-step and proposed two-step Bayesian lassos were executed for 10,000 iterations (after discarding an initial “burn-in” period of 1,000 iterations), which took about 100 seconds on a 2.6 GHz machine for each chain. Further numerical details (such as the initialization of the chains) may be found by direct inspection of the R code, which we provide in its entirety in the Supplementary Material.

We now show that the Markov chain of the proposed two-step Bayesian lasso mixes substantially better than that of the original Bayesian lasso when applied to this gene

expression data set. Specifically, the lag-one autocorrelation of the σ^2 chain for the two-step Bayesian lasso is 0.3885, whereas it is 0.7794 for the original Bayesian lasso. We also computed the effective sample size of the σ^2 chain using the `effectiveSize` function of the R package `coda` (Plummer et al., 2006). The effective sample size is 4,160 for the two-step Bayesian lasso and 1,240 for the original Bayesian lasso. These effective sample sizes essentially demonstrate that the two-step Bayesian lasso needs only about 30% as many Gibbs sampling iterations to obtain an MCMC sample of equivalent quality to that of the original Bayesian lasso. Since the computational time for a single iteration is essentially the same for both algorithms, the two-step Bayesian lasso also requires only about 30% as much time as the original Bayesian lasso to obtain an MCMC sample of equivalent quality. Such considerations are particularly important when considering the high-dimensional data sets to which the lasso and Bayesian lasso are often applied.

Remark. The reader may wonder why we have chosen to examine the autocorrelation and effective sample size of the σ^2 chain instead of the β chain (i.e., the individual β_j chains). The reason is simply that the autocorrelation and effective sample size of the β chain can fail to accurately convey the mixing behavior of regression-type Gibbs samplers. In short, the sampled iterates of certain quadratic forms in β can be very highly autocorrelated even though the β_j chains themselves have an autocorrelation near zero. Such convergence behavior leads to serious inaccuracy when using the MCMC output for uncertainty quantification, which is the very reason why the Bayesian lasso is employed in the first place. In contrast, there are strong theoretical connections between the autocorrelation of the σ^2 chain and the true convergence rate for regression-type Gibbs samplers. See Rajaratnam and Sparks (2015) for a thorough discussion of these concepts.

5.1.2 Results for Spike-and-Slab

Next, we investigate the performance of the two-step Gibbs sampler in (6) relative to the original sampler in (3) using the spike-and-slab prior. Both the original and proposed Gibbs samplers were executed for 10,000 iterations (after discarding an initial “burn-in” period of 1,000 iterations), which took about 80 seconds on a 2.6 GHz machine for each chain. Other numerical details may be found by direct inspection of the R code, which we provide in its entirety in the Supplemental Material.

As was the case with the two-step Bayesian lasso, the blocked version of the spike-and-slab Gibbs sampler exhibits mixing properties that are substantially better than those of the corresponding original sampler. Specifically, the lag-one autocorrelation of the σ^2 chain for the two-step spike-and-slab Gibbs sampler is 0.0187 whereas it is 0.5174 for the original

spike-and-slab Gibbs sampler. Moreover, the effective sample size of the σ^2 chain is 9,372 for the fast spike-and-slab Gibbs sampler and 2,977 for the original spike-and-slab Gibbs sampler. Thus, the blocking approach of the proposed two-step sampler once again yields a sampler that is dramatically more efficient than the original three-step sampler.

5.2 Infrared Spectroscopy Data

We next evaluate the performance of the original three-step and proposed two-step approaches in the context of Bayesian lasso through their application to the infrared spectroscopy data of [Osborne et al. \(1984\)](#) and [Brown et al. \(2001\)](#), which is publicly available as the data set `cookie` in the R package `ppls` ([Kramer et al., 2008](#)). We used the first $n = 40$ observations and the first of the response variables (corresponding to fat content). The $p = 700$ covariates of this data set exhibit high multicollinearity, with a median pairwise correlation of 0.96. The columns of \mathbf{X} were standardized to have mean zero and squared Euclidean norm n . The regularization parameter was taken to be $\lambda = 0.0504$, which yields $\min\{n, p\}/2 = 20$ nonzero coefficients in the lasso estimate. Both the original and two-step Bayesian lassos were executed for 10,000 iterations (after discarding an initial “burn-in” period of 1,000 iterations), which took about 25 minutes on a 2.6 GHz machine for each chain. The R code is provided in the Supplementary Material.

two-stepAs with the gene expression data of the previous subsection, the Markov chain of the two-step Bayesian lasso mixes much better than that of the original Bayesian lasso when applied to this infrared spectroscopy data set. The lag-one autocorrelation of the σ^2 chain is 0.0924 for the fast Bayesian lasso and 0.9560 for the original Bayesian lasso. The effective sample size of the σ^2 chain is 7,790 for the fast Bayesian lasso and 225 for the original Bayesian lasso. two-stepThus, the two-step Bayesian lasso requires only about 3% as many Gibbs sampling iterations to achieve the same effective sample size as the original Bayesian lasso. Hence, the two-step Bayesian lasso requires only about 3% as much time as the original Bayesian lasso to obtain an MCMC sample of equivalent quality. (Also see the previous subsection for further comments on the consideration of the σ^2 chain specifically.)

5.3 Communities and Crime Data

For a third application to real data, we consider the communities and crime data of [Redmond and Baveja \(2002\)](#), which is publicly available through the UC Irvine Machine Learning Repository ([Lichman, 2013](#)) as the Communities and Crime Data Set. We chose 50 covariates from that data set and constructed $p = 1325$ covariates by taking the first-order, quadratic, and multiplicative interaction terms involving those 50 raw covariates. We again illustrate

the performance of the original three-step and proposed two-step chains in the context of the Bayesian lasso model in a small- n , large- p setting. We choose $n = 10$ of the 1994 total observations uniformly at random. Each of the 1325 columns (each of length 10) of the resulting \mathbf{X} matrix were standardized to have mean zero and squared Euclidean norm n . The regularization parameter was taken to be $\lambda = 1.331$, which yields $\min\{n, p\}/2 = 5$ nonzero coefficients in the lasso estimate for the particular observations selected. Both the original and two-step Bayesian lassos were executed for 10,000 iterations (after discarding an initial “burn-in” period of 1,000 iterations), which took about 90 minutes on a 2.6 GHz machine for each chain. The R code is provided in the Supplementary Material.

Once again, the Markov chain of the two-step Bayesian lasso mixes considerably faster than that of the original Bayesian lasso. The lag-one autocorrelation of the σ^2 chain is 0.0017 for the two-step Bayesian lasso and 0.9942 for the original Bayesian lasso. The effective sample size of the σ^2 chain is 10,000 for the two-step Bayesian lasso and 29 for the original Bayesian lasso. (Note that the `effectiveSize` function involves the use of AIC to select the order of an autoregressive model, and obtaining an effective sample size exactly equal to the number of MCMC iterations simply indicates that AIC has selected a trivial autoregressive model of order zero.) Thus, the two-step Bayesian lasso requires only about 0.3% as many Gibbs sampling iterations to achieve the same effective sample size as the original Bayesian lasso. Hence, the two-step Bayesian lasso requires only about 0.3% as much time as the original Bayesian lasso to obtain an MCMC sample of equivalent quality. (Also see the previous subsections for further comments on the consideration of the σ^2 chain specifically.)

Data Set	n	p	Autocorrelation		Effective Size		
			Two-step	Original	Two-step	Original	Ratio
Gene Expr. (Spike-Slab)	120	200	0.0187	0.5174	9,372	2,977	3.15
Gene Expr. (Bayesian lasso)	120	200	0.3885	0.7794	4,160	1,240	3.4
Infrared Spectroscopy	40	700	0.0924	0.9560	7,790	225	34.6
Communities & Crime	10	1,325	0.0017	0.9942	10,000	29	344.8

Table 1: Autocorrelation and effective sample size for the σ^2 chain of the two-step Bayesian lasso and original Bayesian lasso as applied to the three datasets in Section 5. Note that n and p denote (respectively) the sample size and number of covariates for each data set.

5.4 Summary of Applications

The results for all three data sets in this section are summarized in Table 1. It is clear that the two-step chain and the original three-step chain exhibit the same behavior (in regard

to n and p) for these real data sets as for the simulated data sets of Section 4. Specifically, the original three-step chain mixes very slowly when p is large relative to n , as illustrated by the large autocorrelation and small effective sample size of the σ^2 chain. In contrast, the two-step chain enjoys excellent mixing properties in all n and p regimes and becomes better as p gets larger (in fact, there is an unexpected “benefit of dimensionality”).

6 Theoretical Properties

In this section we undertake an investigation into the theoretical convergence and spectral properties of the proposed two-step chain and the original three-step chains. In particular, we investigate whether these Markov chains converge at a geometric rate (geometric ergodicity) and also the specific behavior of their singular values (trace class/Hilbert Schmidt properties). As stated in the introduction, proving geometric ergodicity and trace class/Hilbert Schmidt properties for practical Markov chains such as these can be rather tricky and a matter of art, where each Markov chain requires a genuinely unique analysis based on its specific structure. Hence, we provide results here for the Bayesian lasso model outlined in Section 2.2. A theoretical study of all the other two-step and three-step Markov chains is a big and challenging undertaking, and is the task of ongoing and future research.

We first proceed to establish geometric ergodicity of the two-step Bayesian lasso Gibbs sampler using the method of Rosenthal (1995). This approach provides a quantitative upper bound on the geometric convergence rate. To express this result rigorously, we first define some notation. For every $m \geq 1$, let $F_m(\sigma_0^2, \beta_0)$ denote the distribution of the m th iterate for the two-step Bayesian lasso Gibbs sampler initialized at (β_0, σ_0^2) . Let F denote the stationary distribution of this Markov chain, i.e., the true joint posterior distribution of (β, σ^2) . Finally, let d_{TV} denote total variation distance. Then we have the following result, which we express using notation similar to that of Theorem 2 of Jones and Hobert (2001).

Theorem 2. *Let $0 < \gamma < 1$, $b = ((n+3)p)(16\gamma + (n+3))/(64\gamma)$, and $d > 2b/(1-\gamma)$. Then for any $0 < r < 1$,*

$$d_{\text{TV}}[F_k(\sigma_0^2, \beta_0), F] \leq (1-\varepsilon)^{rk} + \left(\frac{U^r}{\alpha^{1-r}}\right)^k \left(1 + \frac{b}{1-\gamma} + \frac{\lambda \|\beta_0\|_2^2}{\sigma_0^2}\right),$$

for every $k \geq 1$, where $\varepsilon = \exp(-p\sqrt{d})$, $U = 1 + 2(\gamma d + b)$, and $\alpha = (1+d)/(1+2b+\gamma d)$.

The proof of Theorem 2 uses the lemma below, which is proven in the Supplementary Material.

Lemma 3. Let $C_\tau = \tilde{\mathbf{Y}}^\top (\mathbf{I}_n - \mathbf{X} \mathbf{A}_\tau^{-1} \mathbf{X}^\top) \tilde{\mathbf{Y}}$. Then $\|\mathbf{A}_\tau^{-1} \mathbf{X}^\top \tilde{\mathbf{Y}}\|_2^2 / C_\tau \leq \|\boldsymbol{\tau}\|_1 / 4$.

With Lemma 3 in place, we can now prove Theorem 2.

Proof of Theorem 2. We appeal to Theorem 2 of Jones and Hobert (2001) (see also Theorem 12 of Rosenthal, 1995). To apply this result, it is necessary to establish a drift condition and an associated minorization condition. Let $V(\boldsymbol{\beta}, \sigma^2) = \lambda^2 \boldsymbol{\beta}^\top \boldsymbol{\beta} / \sigma^2$. Let $(\boldsymbol{\beta}_0, \sigma_0^2)$ denote the initial value for the blocked Markov chain, and let $(\boldsymbol{\beta}_1, \sigma_1^2)$ denote the first iteration of the chain. Then let E_0 denote expectation conditional on $(\boldsymbol{\beta}_0, \sigma_0^2)$. To establish the drift condition, observe that

$$\begin{aligned} E_0[V(\boldsymbol{\beta}_1, \sigma_1^2)] &= \lambda^2 E_0[\sigma_1^{-2} E(\boldsymbol{\beta}_1^\top \boldsymbol{\beta}_1 \mid \boldsymbol{\tau}_1, \sigma_1^2)] \\ &= \lambda^2 E_0\left[\text{tr}(\mathbf{A}_\tau^{-1}) + \|\mathbf{A}_\tau^{-1} \mathbf{X}^\top \tilde{\mathbf{Y}}\|_2^2 E(\sigma_1^{-2} \mid \boldsymbol{\tau})\right] \\ &= \lambda^2 E_0\left[\text{tr}(\mathbf{A}_\tau^{-1}) + \|\mathbf{A}_\tau^{-1} \mathbf{X}^\top \tilde{\mathbf{Y}}\|_2^2 (n-1)/C_\tau\right] \\ &\leq \lambda^2 E_0[\text{tr}(\mathbf{D}_\tau) + \|\boldsymbol{\tau}\|_1 (n-1)/4] = E_0(\|\boldsymbol{\tau}\|_1) (n+3)\lambda^2/4, \end{aligned} \quad (8)$$

where the inequality is by Lemma 3 and the fact that $\text{tr}(\mathbf{A}_\tau^{-1}) = \text{tr}[(\mathbf{X}^\top \mathbf{X} + \mathbf{D}_\tau^{-1})^{-1}] \leq \text{tr}[(\mathbf{D}_\tau^{-1})^{-1}] = \text{tr}(\mathbf{D}_\tau)$. Then continuing from (8), we have

$$E_0[V(\boldsymbol{\beta}_1, \sigma_1^2)] \leq \frac{(n+3)\lambda^2}{4} \sum_{j=1}^p \left(\frac{|\beta_{0,j}|}{\lambda \sigma_0} + \frac{1}{\lambda^2} \right) = \frac{n+3}{4} \sum_{j=1}^p \frac{\lambda |\beta_{0,j}|}{\sigma_0} + \frac{(n+3)p}{4} \quad (9)$$

by the basic properties of the inverse Gaussian distribution. Now note that $u \leq \delta u^2 + (4\delta)^{-1}$ for all $u \geq 0$ and $\delta > 0$. Applying this result to (9) for each j with $u = \lambda |\beta_{0,j}| / \sigma_0$ and $\delta = 4\gamma / (n+3)$ yields

$$E_0[V(\boldsymbol{\beta}_1, \sigma_1^2)] \leq \gamma \sum_{j=1}^p \frac{\lambda^2 \beta_{0,j}^2}{\sigma_0^2} + \frac{n+3}{4} \left[\frac{(n+3)p}{16\gamma} \right] + \frac{(n+3)p}{4} = \gamma V(\boldsymbol{\beta}_0, \sigma_0^2) + b,$$

establishing the drift condition.

To establish the associated minorization condition, observe that k as defined in (7) is given by

$$\begin{aligned}
& k[(\sigma_0^2, \beta_0), (\beta_1, \sigma_1^2)] \\
&= \int_{\mathbb{R}_+^p} \frac{\lambda^p}{(2\pi)^{p/2}} \exp\left[\frac{\lambda\|\beta_0\|_1}{\sigma_0} - \frac{\beta_0^\top \mathbf{D}_\tau^{-1} \beta_0}{2\sigma_0^2} - \frac{\lambda^2\|\tau\|_1}{2}\right] \prod_{j=1}^p \tau_j^{-1/2} \times \\
&\quad \frac{(C_\tau/2)^{(n-1)/2}}{\Gamma(\frac{n-1}{2}) \sigma_1^{n+1}} \exp\left(-\frac{C_\tau}{2\sigma_1^2}\right) \frac{\det(\mathbf{A}_\tau)^{1/2}}{(2\pi\sigma_1^2)^{p/2}} \exp\left[\frac{1}{2\sigma_1^2} \left\| \mathbf{A}_\tau^{1/2}(\beta_1 - \mathbf{A}_\tau^{-1} \mathbf{X}^\top \tilde{\mathbf{Y}}) \right\|_2^2\right] d\tau \\
&= \int_{\mathbb{R}_+^p} \frac{(\lambda/2\pi)^p}{2^{(n-1)/2} \Gamma(\frac{n-1}{2})} \frac{\det(\mathbf{A}_\tau \mathbf{D}_\tau^{-1})^{1/2} C_\tau^{(n-1)/2}}{\sigma_1^{n+p+1}} \exp\left(-\frac{\lambda^2\|\tau\|_1}{2}\right) \times \\
&\quad \exp\left(-\frac{\|\tilde{\mathbf{Y}} - \mathbf{X}\beta_1\|_2^2}{2\sigma_1^2} - \frac{\beta_1^\top \mathbf{D}_\tau^{-1} \beta_1}{2\sigma_1^2}\right) \exp\left(\frac{\lambda\|\beta_0\|_1}{\sigma_0} - \frac{\beta_0^\top \mathbf{D}_\tau^{-1} \beta_0}{2\sigma_0^2}\right) d\tau. \quad (10)
\end{aligned}$$

Now suppose that $V(\beta_0, \sigma_0^2) \leq d$. Then $\lambda^2 \beta_{0,j}^2 / \sigma_0^2 \leq d$ for each j . Let $\xi = d^{1/2} \lambda^{-1} \mathbf{1}_p$. Then

$$\exp\left(\frac{\lambda\|\beta_0\|_1}{\sigma_0} - \frac{\beta_0^\top \mathbf{D}_\tau^{-1} \beta_0}{2\sigma_0^2}\right) \geq \exp\left(-\frac{\xi^\top \mathbf{D}_\tau^{-1} \xi}{2}\right) = \varepsilon \exp\left(\lambda\|\xi\|_1 - \frac{\xi^\top \mathbf{D}_\tau^{-1} \xi}{2}\right),$$

noting that $\varepsilon = \exp(-\lambda\|\xi\|_1)$. Combining this inequality with (10) yields

$$\begin{aligned}
k[(\beta_0, \sigma_0^2), (\beta_1, \sigma_1^2)] &\geq \int_{\mathbb{R}_+^p} \frac{(\lambda/2\pi)^p \det(\mathbf{A}_\tau \mathbf{D}_\tau^{-1})^{1/2} C_\tau^{(n-1)/2}}{2^{(n-1)/2} \Gamma(\frac{n-1}{2}) \sigma_1^{n+p+1}} \exp\left(-\frac{\lambda^2\|\tau\|_1}{2}\right) \times \\
&\quad \exp\left(-\frac{\|\tilde{\mathbf{Y}} - \mathbf{X}\beta_1\|_2^2}{2\sigma_1^2} - \frac{\beta_1^\top \mathbf{D}_\tau^{-1} \beta_1}{2\sigma_1^2}\right) \varepsilon \exp\left(\lambda\|\xi\|_1 - \frac{\xi^\top \mathbf{D}_\tau^{-1} \xi}{2}\right) d\tau \\
&= \varepsilon k[(\xi, 1), (\beta_1, \sigma_1^2)]
\end{aligned}$$

for all $(\beta, \sigma^2) \in \mathbb{R}^p \times \mathbb{R}_+$. Thus, the minorization condition is established. \square

Note that for Theorem 2 to be useful, the bound must actually decrease with k . Thus, it is necessary to choose r small enough that $U^r / \alpha^{1-r} < 1$. Then for small enough r , the bound is dominated by the term $(1 - \varepsilon)^{rk}$, which is approximately $(1 - r\varepsilon)^k$ for small r and ε . Now observe that $d > 2b > n^2 p / 32$. It follows that

$$1 - r\varepsilon = 1 - r \exp(-p d^{1/2}) > 1 - r \exp(-n p^{3/2} / 32^{1/2}),$$

which tends to 1 exponentially fast as n or p tends to infinity. Thus, although Theorem 2 establishes that the two-step Bayesian lasso Gibbs sampler is geometrically ergodic and

provides a bound for the rate constant, it is not clear how sharp it is. Hence, the bound may not be particularly informative in high-dimensional contexts.

Additional theoretical insight into the differences between the original and blocked sampling schemes may be gained through consideration of the spectral properties of the two Gibbs samplers. The following theorem provides a key difference between these two chains.

Theorem 4. *The Markov operator corresponding to the original three-step Gibbs transition density \hat{k} is not Hilbert-Schmidt, while the Markov operator corresponding to the blocked Gibbs transition density k is trace class (and hence Hilbert-Schmidt) for all possible values of p and n .*

The proof of this result is quite technical and long and may be found in the Supplementary Material. As discussed in the introduction, the above result implies that the eigenvalues of the absolute value of the non-self-adjoint operator associated with the original Gibbs chain are not square-summable. In contrast, it also implies that the eigenvalues of the self-adjoint and positive operator corresponding to the blocked Gibbs chain are summable (which implies square-summability, as these eigenvalues are bounded by 1). Based on this result, we would expect the blocked Gibbs chain to be more efficient than the original Gibbs chain. The numerical results (for high-dimensional regimes) provided in Sections 4 and 5 confirm this assertion.

Supplementary Material

This supplementary material is organized as follows. Section S1 contains proofs of Lemmas 1 and 3 and Theorem 4. Section S2 contains additional numerical results. Section S3 contains details of the numerical results in Sections 4 and 5. Section S4 contains R code for executing both the original and two-step Bayesian lasso algorithms. In addition, the R code for generating the numerical results of Sections 4, 5, and S2 is provided in its entirety in an accompanying file. Supplementary material comprises proofs of Lemmas 1 and 3 and Theorem 4, additional numerical results, and details of the numerical results in Section 4.

S1 Proofs

Proof of Lemma 1. Integrating out β from the joint posterior $\pi(\beta, \sigma^2, \tau \mid \mathbf{Y})$ yields

$$\begin{aligned}
 \pi(\sigma^2, \tau \mid \mathbf{Y}) &= \int \pi(\beta, \sigma^2, \tau \mid \mathbf{Y}) d\beta \\
 &= \frac{(\lambda^2/2)^p}{(2\pi\sigma^2)^{(n+p+1)/2}} \exp\left(-\frac{\lambda^2}{2} \sum_{j=1}^p \tau_j\right) \\
 &\quad \times \int \exp\left[-\frac{1}{2\sigma^2} \left(\|\tilde{\mathbf{Y}} - \mathbf{X}\beta\|_2^2 + \|\mathbf{D}_\tau^{-1/2}\beta\|_2^2\right)\right] d\beta \\
 &= \frac{(\lambda^2/2)^p}{(2\pi\sigma^2)^{(n+p+1)/2}} \exp\left[-\frac{\lambda^2\|\tau\|_1}{2} - \frac{1}{2\sigma^2} \tilde{\mathbf{Y}}^\top (\mathbf{I}_n - \mathbf{X}\mathbf{A}_\tau^{-1}\mathbf{X}^\top) \tilde{\mathbf{Y}}\right] \\
 &\quad \times \int \exp\left[-\frac{1}{2\sigma^2} \left\|\mathbf{A}_\tau^{1/2}(\beta - \mathbf{A}_\tau^{-1}\mathbf{X}^\top\tilde{\mathbf{Y}})\right\|_2^2\right] d\beta \\
 &= \frac{(\lambda^2/2)^p}{(2\pi\sigma^2)^{(n+p+1)/2} \det(\mathbf{A}_\tau)^{1/2}} \exp\left[-\frac{\lambda^2\|\tau\|_1}{2} - \frac{\tilde{\mathbf{Y}}^\top (\mathbf{I}_n - \mathbf{X}\mathbf{A}_\tau^{-1}\mathbf{X}^\top) \tilde{\mathbf{Y}}}{2\sigma^2}\right].
 \end{aligned}$$

Then it is clear that

$$\pi(\sigma^2 \mid \tau, \mathbf{Y}) \propto \frac{1}{(\sigma^2)^{(n+p+1)/2}} \exp\left[-\frac{\tilde{\mathbf{Y}}^\top (\mathbf{I}_n - \mathbf{X}\mathbf{A}_\tau^{-1}\mathbf{X}^\top) \tilde{\mathbf{Y}}}{2\sigma^2}\right],$$

and the result follows immediately. \square

Proof of Lemma 3. Let $\mathbf{X} = \mathbf{U}\mathbf{\Omega}\mathbf{V}^T$ be a singular value decomposition of \mathbf{X} , where $\omega_1, \dots, \omega_{\min\{n,p\}}$ are the the singular values, and let $\tau_{\max} = \max_{1 \leq j \leq p} \tau_j$. Then

$$\begin{aligned} \frac{\|\mathbf{A}_\tau^{-1}\mathbf{X}^T\tilde{\mathbf{Y}}\|_2^2}{C_\tau} &= \frac{\tilde{\mathbf{Y}}^T\mathbf{U}\mathbf{\Omega}\mathbf{V}^T(\mathbf{V}\mathbf{\Omega}^T\mathbf{\Omega}\mathbf{V}^T + \mathbf{D}_\tau^{-1})^{-2}\mathbf{V}\mathbf{\Omega}^T\mathbf{U}^T\tilde{\mathbf{Y}}}{\tilde{\mathbf{Y}}^T\tilde{\mathbf{Y}} - \tilde{\mathbf{Y}}^T\mathbf{U}\mathbf{\Omega}\mathbf{V}^T(\mathbf{V}\mathbf{\Omega}^T\mathbf{\Omega}\mathbf{V}^T + \mathbf{D}_\tau^{-1})^{-1}\mathbf{V}\mathbf{\Omega}^T\mathbf{U}^T\tilde{\mathbf{Y}}} \\ &\leq \frac{\tilde{\mathbf{Y}}^T\mathbf{U}\mathbf{\Omega}\mathbf{V}^T(\mathbf{V}\mathbf{\Omega}^T\mathbf{\Omega}\mathbf{V}^T + \tau_{\max}^{-1}\mathbf{I}_p)^{-2}\mathbf{V}\mathbf{\Omega}^T\mathbf{U}^T\tilde{\mathbf{Y}}}{\tilde{\mathbf{Y}}^T\tilde{\mathbf{Y}} - \tilde{\mathbf{Y}}^T\mathbf{U}\mathbf{\Omega}\mathbf{V}^T(\mathbf{V}\mathbf{\Omega}^T\mathbf{\Omega}\mathbf{V}^T + \tau_{\max}^{-1}\mathbf{I}_p)^{-1}\mathbf{V}\mathbf{\Omega}^T\mathbf{U}^T\tilde{\mathbf{Y}}} \\ &= \frac{\tilde{\mathbf{Y}}^T\mathbf{U}\mathbf{\Omega}(\mathbf{\Omega}^T\mathbf{\Omega} + \tau_{\max}^{-1}\mathbf{I}_p)^{-2}\mathbf{\Omega}^T\mathbf{U}^T\tilde{\mathbf{Y}}}{\tilde{\mathbf{Y}}^T\mathbf{U}\mathbf{U}^T\tilde{\mathbf{Y}} - \tilde{\mathbf{Y}}^T\mathbf{U}\mathbf{\Omega}(\mathbf{\Omega}^T\mathbf{\Omega} + \tau_{\max}^{-1}\mathbf{I}_p)^{-1}\mathbf{\Omega}^T\mathbf{U}^T\tilde{\mathbf{Y}}} = \frac{\tilde{\mathbf{Y}}_\star^T \mathbf{G} \tilde{\mathbf{Y}}_\star}{\tilde{\mathbf{Y}}_\star^T \mathbf{H} \tilde{\mathbf{Y}}_\star}, \end{aligned}$$

where $\tilde{\mathbf{Y}}_\star = \mathbf{U}^T\tilde{\mathbf{Y}}$ and

$$\mathbf{G} = \text{Diag}\left[\frac{\omega_1^2}{(\omega_1^2 + \tau_{\max}^{-1})^2}, \dots, \frac{\omega_n^2}{(\omega_n^2 + \tau_{\max}^{-1})^2}\right], \quad \mathbf{H} = \text{Diag}\left(\frac{\tau_{\max}^{-1}}{\omega_1^2 + \tau_{\max}^{-1}}, \dots, \frac{\tau_{\max}^{-1}}{\omega_n^2 + \tau_{\max}^{-1}}\right),$$

taking $\omega_i = 0$ for all $i > p$ if $n > p$. Then it is clear that

$$\begin{aligned} \frac{\|\mathbf{A}_\tau^{-1}\mathbf{X}^T\tilde{\mathbf{Y}}\|_2^2}{C_\tau} &\leq \max_{1 \leq i \leq n} \left[\frac{\omega_i^2}{(\omega_i^2 + \tau_{\max}^{-1})^2} \left(\frac{\tau_{\max}^{-1}}{\omega_i^2 + \tau_{\max}^{-1}} \right)^{-1} \right] \\ &\leq \max_{1 \leq i \leq n} \left[\frac{1}{4\tau_{\max}^{-1}} \left(\frac{\tau_{\max}^{-1}}{\omega_i^2 + \tau_{\max}^{-1}} \right)^{-1} \right] \leq \frac{\tau_{\max}}{4} \leq \frac{\|\boldsymbol{\tau}\|_1}{4}, \end{aligned}$$

noting for the second inequality that $a/(a+b)^2 \leq 1/(4b)$ for all $a \geq 0$ and $b > 0$. \square

Proof of Theorem 4. Let \hat{K} be the Markov operator associated with the density \hat{k} . Let \hat{K}^* denote the adjoint of \hat{K} . Note that \hat{K} is Hilbert-Schmidt if and only if $\hat{K}^*\hat{K}$ is trace class, which happens if and only if $I < \infty$ (see [Jorgens, 1982](#)) where

$$\begin{aligned} I &:= \int_{\mathbb{R}^p} \int_{\mathbb{R}_+} \int_{\mathbb{R}^p} \int_{\mathbb{R}_+} \hat{k}\left((\boldsymbol{\beta}, \sigma^2), (\tilde{\boldsymbol{\beta}}, \tilde{\sigma}^2)\right) \hat{k}^*\left((\tilde{\boldsymbol{\beta}}, \tilde{\sigma}^2), (\boldsymbol{\beta}, \sigma^2)\right) d\boldsymbol{\beta} d\sigma^2 d\tilde{\boldsymbol{\beta}} d\tilde{\sigma}^2 \\ &= \int_{\mathbb{R}^p} \int_{\mathbb{R}_+} \int_{\mathbb{R}^p} \int_{\mathbb{R}_+} \hat{k}^2\left((\boldsymbol{\beta}, \sigma^2), (\tilde{\boldsymbol{\beta}}, \tilde{\sigma}^2)\right) \frac{f(\boldsymbol{\beta}, \sigma^2 | \mathbf{Y})}{f(\tilde{\boldsymbol{\beta}}, \tilde{\sigma}^2 | \mathbf{Y})} d\boldsymbol{\beta} d\sigma^2 d\tilde{\boldsymbol{\beta}} d\tilde{\sigma}^2. \end{aligned} \quad (\text{S11})$$

By (4), we get that

$$\begin{aligned}
& \hat{k}^2 \left((\beta, \sigma^2), (\tilde{\beta}, \tilde{\sigma}^2) \right) \\
&= \left[\int_{\mathbb{R}_+^p} f(\tilde{\sigma}^2 | \tilde{\beta}, \tau, \mathbf{Y}) f(\tilde{\beta} | \tau, \sigma^2, \mathbf{Y}) f(\tau | \beta, \sigma^2, \mathbf{Y}) d\tau \right]^2 \\
&= \int_{\mathbb{R}_+^p} \int_{\mathbb{R}_+^p} f(\tilde{\sigma}^2 | \tilde{\beta}, \tau, \mathbf{Y}) f(\tilde{\beta} | \tau, \sigma^2, \mathbf{Y}) f(\tau | \beta, \sigma^2, \mathbf{Y}) \\
&\quad f(\tilde{\sigma}^2 | \tilde{\beta}, \tilde{\tau}, \mathbf{Y}) f(\tilde{\beta} | \tilde{\tau}, \sigma^2, \mathbf{Y}) f(\tilde{\tau} | \beta, \sigma^2, \mathbf{Y}) d\tau d\tilde{\tau}.
\end{aligned}$$

It follows from (S11) and Fubini's theorem that

$$\begin{aligned}
I &= \int_{\mathbb{R}_+^p} \int_{\mathbb{R}_+^p} \int_{\mathbb{R}^p} \int_{\mathbb{R}_+} \int_{\mathbb{R}^p} \int_{\mathbb{R}_+} f(\tilde{\sigma}^2 | \tilde{\beta}, \tau, \mathbf{Y}) f(\tilde{\beta} | \tau, \sigma^2, \mathbf{Y}) f(\tau | \beta, \sigma^2, \mathbf{Y}) \\
&\quad f(\tilde{\sigma}^2 | \tilde{\beta}, \tilde{\tau}, \mathbf{Y}) f(\tilde{\beta} | \tilde{\tau}, \sigma^2, \mathbf{Y}) f(\tilde{\tau} | \beta, \sigma^2, \mathbf{Y}) \frac{f(\beta, \sigma^2 | \mathbf{Y})}{f(\tilde{\beta}, \tilde{\sigma}^2 | \mathbf{Y})} \\
&\quad d\tau d\tilde{\tau} d\beta d\sigma^2 d\tilde{\beta} d\tilde{\sigma}^2.
\end{aligned}$$

A straightforward manipulation of conditional densities shows that

$$\begin{aligned}
& f(\tilde{\sigma}^2 | \tilde{\beta}, \tilde{\tau}, \mathbf{Y}) f(\tilde{\beta} | \tilde{\tau}, \sigma^2, \mathbf{Y}) f(\tilde{\tau} | \beta, \sigma^2, \mathbf{Y}) \frac{f(\beta, \sigma^2 | \mathbf{Y})}{f(\tilde{\beta}, \tilde{\sigma}^2 | \mathbf{Y})} \\
&= f(\beta | \tilde{\tau}, \sigma^2, \mathbf{Y}) f(\sigma^2 | \tilde{\beta}, \tilde{\tau}, \mathbf{Y}) f(\tilde{\tau} | \tilde{\beta}, \tilde{\sigma}^2, \mathbf{Y}).
\end{aligned}$$

It follows that

$$\begin{aligned}
I &= \int_{\mathbb{R}_+} \int_{\mathbb{R}_+} \int_{\mathbb{R}^p} \int_{\mathbb{R}^p} \int_{\mathbb{R}_+^p} \int_{\mathbb{R}_+^p} f(\tilde{\sigma}^2 | \tilde{\beta}, \tau, \mathbf{Y}) f(\tilde{\beta} | \tau, \sigma^2, \mathbf{Y}) f(\tau | \beta, \sigma^2, \mathbf{Y}) \\
&\quad f(\beta | \tilde{\tau}, \sigma^2, \mathbf{Y}) f(\sigma^2 | \tilde{\beta}, \tilde{\tau}, \mathbf{Y}) f(\tilde{\tau} | \tilde{\beta}, \tilde{\sigma}^2, \mathbf{Y}) d\sigma^2 d\tilde{\sigma}^2 d\beta d\tilde{\beta} d\tau d\tilde{\tau} \quad (\text{S12})
\end{aligned}$$

For convenience, we introduce and use the following notation in the subsequent proof.

$$\begin{aligned}
\hat{\beta} &= \mathbf{A}_\tau^{-1} X^T \mathbf{Y} & \hat{\beta}_* &= \mathbf{A}_{\tilde{\tau}}^{-1} X^T \mathbf{Y} \\
\Delta_1 &= (\tilde{\beta} - \hat{\beta})^T \mathbf{A}_\tau (\tilde{\beta} - \hat{\beta}) & \Delta_{1*} &= (\beta - \hat{\beta}_*)^T \mathbf{A}_{\tilde{\tau}} (\beta - \hat{\beta}_*) \\
\tilde{\Delta} &= (\mathbf{Y} - X\tilde{\beta})^T (\mathbf{Y} - X\tilde{\beta}) + \tilde{\beta}^T D_\tau^{-1} \tilde{\beta} + 2\xi & \tilde{\Delta}_* &= (\mathbf{Y} - X\tilde{\beta})^T (\mathbf{Y} - X\tilde{\beta}) + \tilde{\beta}^T D_{\tilde{\tau}}^{-1} \tilde{\beta} + 2\xi.
\end{aligned} \tag{S13}$$

By (3) we get that

$$\begin{aligned}
& f(\tilde{\sigma}^2 \mid \tilde{\beta}, \tau, \mathbf{Y}) f(\tilde{\beta} \mid \tau, \sigma^2, \mathbf{Y}) f(\tau \mid \beta, \sigma^2, \mathbf{Y}) f(\beta \mid \tilde{\tau}, \sigma^2, \mathbf{Y}) \times \\
& f(\sigma^2 \mid \tilde{\beta}, \tilde{\tau}, \mathbf{Y}) f(\tilde{\tau} \mid \tilde{\beta}, \tilde{\sigma}^2, \mathbf{Y}) \\
= & C_3 \left\{ \frac{\tilde{\Delta}^{\frac{n+p+2\alpha}{2}} \exp(-\tilde{\Delta}/(2\tilde{\sigma}^2))}{(\tilde{\sigma}^2)^{\frac{n+p+2\alpha}{2}+1}} \right\} \left\{ \frac{|\mathbf{A}_\tau|^{\frac{1}{2}} \exp(-\Delta_1/(2\sigma^2))}{\sigma^p} \right\} \times \\
& \left\{ \prod_{j=1}^p (\tau_j)^{-\frac{1}{2}} \exp\left(-\frac{\beta_j^2}{2\sigma^2\tau_j} + \frac{\lambda}{\sigma}|\beta_j| - \frac{1}{2}\lambda^2\tau_j\right) \right\} \left\{ \frac{|\mathbf{A}_{\tilde{\tau}}|^{\frac{1}{2}} \exp(-\Delta_{1*}/(2\sigma^2))}{\sigma^p} \right\} \times \\
& \left\{ \frac{\tilde{\Delta}_*^{\frac{n+p+2\alpha}{2}} \exp(-\tilde{\Delta}_*/(2\sigma^2))}{(\sigma^2)^{\frac{n+p+2\alpha}{2}+1}} \right\} \times \left\{ \prod_{j=1}^p (\tilde{\tau}_j)^{-\frac{1}{2}} \exp\left(-\frac{\tilde{\beta}_j^2}{2\tilde{\sigma}^2\tilde{\tau}_j} + \frac{\lambda}{\tilde{\sigma}}|\tilde{\beta}_j| - \frac{1}{2}\lambda^2\tilde{\tau}_j\right) \right\} \\
\geq & C_3 f_1(\tau, \tilde{\tau}) \left\{ \frac{\tilde{\Delta}^{\frac{n+p+2\alpha}{2}} \exp\left(-\frac{\tilde{\Delta} + \tilde{\beta}^T D_{\tilde{\tau}}^{-1} \tilde{\beta}}{2\tilde{\sigma}^2}\right)}{(\tilde{\sigma}^2)^{\frac{n+p+2\alpha}{2}+1}} \right\} \left\{ \frac{\tilde{\Delta}_*^{\frac{n+p+2\alpha}{2}} \exp\left(-\frac{\Delta_1 + \Delta_{1*} + \tilde{\Delta}_* + \beta^T D_{\tau}^{-1} \beta}{2\sigma^2}\right)}{(\sigma^2)^{\frac{n+p+2\alpha}{2}+p+1}} \right\} \quad (\text{S14})
\end{aligned}$$

where

$$C_3 = \lambda^{2p} \left[(2\pi)^p 2^{\frac{n+p+2\alpha}{2}} \Gamma\left(\frac{n+p+2\alpha}{2}\right) \right]^{-2}$$

and

$$f_1(\tau, \tilde{\tau}) = \left\{ \prod_{j=1}^p (\tau_j)^{-\frac{1}{2}} \exp\left(-\frac{\lambda^2\tau_j}{2}\right) \right\} \left\{ \prod_{j=1}^p (\tilde{\tau}_j)^{-\frac{1}{2}} \exp\left(-\frac{\lambda^2\tilde{\tau}_j}{2}\right) \right\} |\mathbf{A}_\tau|^{\frac{1}{2}} |\mathbf{A}_{\tilde{\tau}}|^{\frac{1}{2}}.$$

It follows by (S14) and the form of the Inverse-Gamma density that

$$\begin{aligned}
& \int_{\mathbb{R}_+} \int_{\mathbb{R}_+} f(\tilde{\sigma}^2 \mid \tilde{\beta}, \tau, \mathbf{Y}) f(\tilde{\beta} \mid \tau, \sigma^2, \mathbf{Y}) f(\tau \mid \beta, \sigma^2, \mathbf{Y}) \times \\
& f(\beta \mid \tilde{\tau}, \sigma^2, \mathbf{Y}) f(\sigma^2 \mid \tilde{\beta}, \tilde{\tau}, \mathbf{Y}) f(\tilde{\tau} \mid \tilde{\beta}, \tilde{\sigma}^2, \mathbf{Y}) d\sigma^2 d\tilde{\sigma}^2 \\
\geq & C_4 f_1(\tau, \tilde{\tau}) \left\{ \frac{\tilde{\Delta}^{\frac{n+p+2\alpha}{2}}}{\left[\tilde{\Delta} + \tilde{\beta}^T D_{\tilde{\tau}}^{-1} \tilde{\beta}\right]^{\frac{n+p+2\alpha}{2}}} \right\} \left\{ \frac{\tilde{\Delta}_*^{\frac{n+p+2\alpha}{2}}}{\left[\Delta_1 + \Delta_{1*} + \tilde{\Delta}_* + \beta^T D_{\tau}^{-1} \beta\right]^{\frac{n+p+2\alpha}{2}+p}} \right\} \quad (\text{S15})
\end{aligned}$$

where

$$C_4 = 2^{n+2p+2\alpha} \Gamma\left(\frac{n+p+2\alpha}{2}\right)^2 C_3.$$

Note that

$$\begin{aligned}
\Delta_{1*} + \beta^T D_{\tau}^{-1} \beta &= (\beta - \hat{\beta}_*)^T \mathbf{A}_{\tilde{\tau}} (\beta - \hat{\beta}_*) + \beta^T D_{\tau}^{-1} \beta \\
&= (\beta - \hat{\beta}_{**})^T (X^T X + D_{\tilde{\tau}}^{-1} + D_{\tau}^{-1}) (\beta - \hat{\beta}_{**}) + \\
&\quad (\hat{\beta}_{**} - \hat{\beta}_*)^T \mathbf{A}_{\tilde{\tau}} (\hat{\beta}_{**} - \hat{\beta}_*) + \hat{\beta}_{**}^T D_{\tau}^{-1} \hat{\beta}_{**} \\
&= f_2(\tau, \tilde{\tau}) + (\beta - \hat{\beta}_{**})^T (X^T X + D_{\tilde{\tau}}^{-1} + D_{\tau}^{-1}) (\beta - \hat{\beta}_{**}), \quad (\text{S16})
\end{aligned}$$

where $\hat{\beta}_{**} = (X^T X + D_{\tilde{\tau}}^{-1} + D_{\tau}^{-1})^{-1} X^T \mathbf{Y}$ and

$$f_2(\tau, \tilde{\tau}) = (\hat{\beta}_{**} - \hat{\beta}_*)^T \mathbf{A}_{\tilde{\tau}} (\hat{\beta}_{**} - \hat{\beta}_*) + \hat{\beta}_{**}^T D_{\tau}^{-1} \hat{\beta}_{**}.$$

Hence, by (S16) and the form of the multivariate t -distribution (see Kotz and Nadarajah, 2004, for example), we obtain that

$$\begin{aligned}
&\int_{\mathbb{R}^p} \frac{1}{\left[\Delta_1 + \Delta_{1*} + \tilde{\Delta}_* + \beta^T D_{\tau}^{-1} \beta \right]^{\frac{n+p+2\alpha}{2} + p}} d\beta \\
&= \int_{\mathbb{R}^p} \frac{1}{\left[\Delta_1 + \tilde{\Delta}_* + f_2(\tau, \tilde{\tau}) + (\beta - \hat{\beta}_{**})^T (X^T X + D_{\tilde{\tau}}^{-1} + D_{\tau}^{-1}) (\beta - \hat{\beta}_{**}) \right]^{\frac{p+(n+2p+2\alpha)}{2}}} d\beta \\
&= \frac{\Gamma\left(\frac{n+2p+2\alpha}{2}\right) \sqrt{\pi^p} |X^T X + D_{\tilde{\tau}}^{-1} + D_{\tau}^{-1}|^{-\frac{1}{2}}}{\Gamma\left(\frac{n+p+2\alpha}{2} + p\right) \left[\Delta_1 + \tilde{\Delta}_* + f_2(\tau, \tilde{\tau}) \right]^{\frac{n+p+2\alpha}{2} + \frac{p}{2}}}. \quad (\text{S17})
\end{aligned}$$

It follows from (S15) and (S17) that

$$\begin{aligned}
&\int_{\mathbb{R}_+} \int_{\mathbb{R}_+} \int_{\mathbb{R}^p} f(\tilde{\sigma}^2 | \tilde{\beta}, \tau, \mathbf{Y}) f(\tilde{\beta} | \tau, \sigma^2, \mathbf{Y}) f(\tau | \beta, \sigma^2, \mathbf{Y}) \times \\
&\quad f(\beta | \tilde{\tau}, \sigma^2, \mathbf{Y}) f(\sigma^2 | \tilde{\beta}, \tilde{\tau}, \mathbf{Y}) f(\tilde{\tau} | \tilde{\beta}, \tilde{\sigma}^2, \mathbf{Y}) d\sigma^2 d\tilde{\sigma}^2 d\beta \\
&\geq C_4 f_1(\tau, \tilde{\tau}) \left\{ \frac{\tilde{\Delta}^{\frac{n+p+2\alpha}{2}} \tilde{\Delta}_*^{\frac{n+p+2\alpha}{2}}}{\left[\tilde{\Delta} + \tilde{\beta}^T D_{\tilde{\tau}}^{-1} \tilde{\beta} \right]^{\frac{n+p+2\alpha}{2}}} \right\} \left\{ \frac{\Gamma\left(\frac{n+2p+2\alpha}{2}\right) \sqrt{\pi^p} |X^T X + D_{\tilde{\tau}}^{-1} + D_{\tau}^{-1}|^{-\frac{1}{2}}}{\Gamma\left(\frac{n+p+2\alpha}{2} + p\right) \left[\Delta_1 + \tilde{\Delta}_* + f_2(\tau, \tilde{\tau}) \right]^{\frac{n+p+2\alpha}{2} + \frac{p}{2}}} \right\}. \quad (\text{S18})
\end{aligned}$$

Note that

$$\frac{\tilde{\beta}^T D_{\tilde{\tau}}^{-1} \tilde{\beta}}{\tilde{\Delta}} = \frac{\tilde{\beta}^T D_{\tilde{\tau}}^{-1} \tilde{\beta}}{(\mathbf{Y} - X\tilde{\beta})^T (\mathbf{Y} - X\tilde{\beta}) + \tilde{\beta}^T D_{\tilde{\tau}}^{-1} \tilde{\beta} + 2\xi} \leq \frac{\tilde{\beta}^T D_{\tilde{\tau}}^{-1} \tilde{\beta}}{\tilde{\beta}^T D_{\tilde{\tau}}^{-1} \tilde{\beta}} \leq \max_{1 \leq j \leq p} \left(\frac{\tau_j}{\tilde{\tau}_j} \right), \quad (\text{S19})$$

and

$$\begin{aligned}
\frac{\Delta_1}{\tilde{\Delta}_*} &= \frac{(\tilde{\beta} - \hat{\beta})^T (\mathbf{A}_\tau) (\tilde{\beta} - \hat{\beta})}{(\mathbf{Y} - X\tilde{\beta})^T (\mathbf{Y} - X\tilde{\beta}) + \tilde{\beta}^T D_{\tilde{\tau}}^{-1} \tilde{\beta} + 2\xi} \\
&\leq \frac{(\tilde{\beta} - \hat{\beta})^T (\mathbf{A}_\tau) (\tilde{\beta} - \hat{\beta}) + \hat{\beta}^T D_{\tilde{\tau}}^{-1} \hat{\beta} + (\mathbf{Y} - X\hat{\beta})^T (\mathbf{Y} - X\hat{\beta})}{(\mathbf{Y} - X\tilde{\beta})^T (\mathbf{Y} - X\tilde{\beta}) + \tilde{\beta}^T D_{\tilde{\tau}}^{-1} \tilde{\beta} + 2\xi} \\
&= \frac{(\mathbf{Y} - X\tilde{\beta})^T (\mathbf{Y} - X\tilde{\beta}) + \tilde{\beta}^T D_{\tilde{\tau}}^{-1} \tilde{\beta}}{(\mathbf{Y} - X\tilde{\beta})^T (\mathbf{Y} - X\tilde{\beta}) + \tilde{\beta}^T D_{\tilde{\tau}}^{-1} \tilde{\beta} + 2\xi} \\
&\leq 1 + \frac{\tilde{\beta}^T D_{\tilde{\tau}}^{-1} \tilde{\beta}}{\tilde{\beta}^T D_{\tilde{\tau}}^{-1} \tilde{\beta}} \\
&\leq 1 + \max_{1 \leq j \leq p} \left(\frac{\tilde{\tau}_j}{\tau_j} \right). \tag{S20}
\end{aligned}$$

From (S18), (S19), (S20), and the fact

$$\tilde{\Delta}_* = (\mathbf{Y} - X\tilde{\beta})^T (\mathbf{Y} - X\tilde{\beta}) + \tilde{\beta}^T D_{\tilde{\tau}}^{-1} \tilde{\beta} + 2\xi \geq \hat{\beta}_*^T D_{\tilde{\tau}}^{-1} \hat{\beta}_* + (\mathbf{Y} - X\hat{\beta}_*)^T (\mathbf{Y} - X\hat{\beta}_*) + 2\xi$$

($\hat{\beta}_*$ minimizes the L.H.S. as a function of $\tilde{\beta}$), it follows that

$$\begin{aligned}
&\int_{\mathbb{R}^p} \int_{\mathbb{R}_+} \int_{\mathbb{R}_+} f(\tilde{\sigma}^2 | \tilde{\beta}, \tau, \mathbf{Y}) f(\tilde{\beta} | \tau, \sigma^2, \mathbf{Y}) f(\tau | \beta, \sigma^2, \mathbf{Y}) \\
&\quad f(\beta | \tilde{\tau}, \sigma^2, \mathbf{Y}) f(\sigma^2 | \tilde{\beta}, \tilde{\tau}, \mathbf{Y}) f(\tilde{\tau} | \tilde{\beta}, \tilde{\sigma}^2, \mathbf{Y}) d\sigma^2 d\tilde{\sigma}^2 d\beta \\
&\geq f_3(\tau, \tilde{\tau}) \left\{ \frac{1}{\left[\Delta_1 + \tilde{\Delta}_* + f_2(\tau, \tilde{\tau}) \right]^{\frac{p}{2}}} \right\}, \tag{S21}
\end{aligned}$$

where

$$\begin{aligned}
f_3(\tau, \tilde{\tau}) &= C_4 f_1(\tau, \tilde{\tau}) \left\{ \frac{\Gamma\left(\frac{n+2p+2\alpha}{2}\right) \sqrt{\pi^p} |X^T X + D_{\tilde{\tau}}^{-1} + D_{\tau}^{-1}|^{-\frac{1}{2}}}{\Gamma\left(\frac{n+p+2\alpha}{2} + p\right) \left[1 + \max_{1 \leq j \leq p} \left(\frac{\tau_j}{\tilde{\tau}_j}\right)\right]^{\frac{n+p+2\alpha}{2}}} \right\} \times \\
&\quad \left[2 + \max_{1 \leq j \leq p} \left(\frac{\tilde{\tau}_j}{\tau_j}\right) + \frac{f_2(\tau, \tilde{\tau})}{\hat{\beta}_*^T D_{\tilde{\tau}}^{-1} \hat{\beta}_* + (\mathbf{Y} - X\hat{\beta}_*)^T (\mathbf{Y} - X\hat{\beta}_*) + 2\xi} \right]^{-\frac{n+p+2\alpha}{2}}.
\end{aligned}$$

Now, note that

$$\begin{aligned}
& \Delta_1 + \tilde{\Delta}_* + f_2(\boldsymbol{\tau}, \tilde{\boldsymbol{\tau}}) \\
&= (\tilde{\boldsymbol{\beta}} - \hat{\boldsymbol{\beta}})^T (\mathbf{A}_\tau) (\tilde{\boldsymbol{\beta}} - \hat{\boldsymbol{\beta}}) + (\mathbf{Y} - X\tilde{\boldsymbol{\beta}})^T (\mathbf{Y} - X\tilde{\boldsymbol{\beta}}) + \tilde{\boldsymbol{\beta}}^T D_{\tilde{\boldsymbol{\tau}}}^{-1} \tilde{\boldsymbol{\beta}} + 2\xi + f_2(\boldsymbol{\tau}, \tilde{\boldsymbol{\tau}}) \\
&= (\tilde{\boldsymbol{\beta}} - \hat{\boldsymbol{\beta}})^T (\mathbf{A}_\tau) (\tilde{\boldsymbol{\beta}} - \hat{\boldsymbol{\beta}}) + (\tilde{\boldsymbol{\beta}} - \hat{\boldsymbol{\beta}}_*)^T \mathbf{A}_{\tilde{\boldsymbol{\tau}}} (\tilde{\boldsymbol{\beta}} - \hat{\boldsymbol{\beta}}_*) + \\
&\quad (\mathbf{Y} - X\hat{\boldsymbol{\beta}}_*)^T (\mathbf{Y} - X\hat{\boldsymbol{\beta}}_*) + \hat{\boldsymbol{\beta}}_*^T D_{\tilde{\boldsymbol{\tau}}}^{-1} \hat{\boldsymbol{\beta}}_* + 2\xi + f_2(\boldsymbol{\tau}, \tilde{\boldsymbol{\tau}}) \\
&= (\tilde{\boldsymbol{\beta}} - \hat{\boldsymbol{\beta}}_{***})^T (\mathbf{A}_\tau + \mathbf{A}_{\tilde{\boldsymbol{\tau}}}) (\tilde{\boldsymbol{\beta}} - \hat{\boldsymbol{\beta}}_{***}) + \\
&\quad (\hat{\boldsymbol{\beta}}_{***} - \hat{\boldsymbol{\beta}})^T (\mathbf{A}_\tau) (\hat{\boldsymbol{\beta}}_{***} - \hat{\boldsymbol{\beta}}) + (\hat{\boldsymbol{\beta}}_{***} - \hat{\boldsymbol{\beta}}_*)^T \mathbf{A}_{\tilde{\boldsymbol{\tau}}} (\hat{\boldsymbol{\beta}}_{***} - \hat{\boldsymbol{\beta}}_*) + \\
&\quad (\mathbf{Y} - X\hat{\boldsymbol{\beta}}_*)^T (\mathbf{Y} - X\hat{\boldsymbol{\beta}}_*) + \hat{\boldsymbol{\beta}}_*^T D_{\tilde{\boldsymbol{\tau}}}^{-1} \hat{\boldsymbol{\beta}}_* + 2\xi + f_2(\boldsymbol{\tau}, \tilde{\boldsymbol{\tau}}) \\
&= (\tilde{\boldsymbol{\beta}} - \hat{\boldsymbol{\beta}}_{***})^T (\mathbf{A}_\tau + \mathbf{A}_{\tilde{\boldsymbol{\tau}}}) (\tilde{\boldsymbol{\beta}} - \hat{\boldsymbol{\beta}}_{***}) + f_4(\boldsymbol{\tau}, \tilde{\boldsymbol{\tau}}),
\end{aligned}$$

where $\hat{\boldsymbol{\beta}}_{***} = (\mathbf{A}_\tau + \mathbf{A}_{\tilde{\boldsymbol{\tau}}})^{-1} 2X^T \mathbf{Y}$, and

$$\begin{aligned}
f_4(\boldsymbol{\tau}, \tilde{\boldsymbol{\tau}}) &= (\hat{\boldsymbol{\beta}}_{***} - \hat{\boldsymbol{\beta}})^T (\mathbf{A}_\tau) (\hat{\boldsymbol{\beta}}_{***} - \hat{\boldsymbol{\beta}}) + (\hat{\boldsymbol{\beta}}_{***} - \hat{\boldsymbol{\beta}}_*)^T \mathbf{A}_{\tilde{\boldsymbol{\tau}}} (\hat{\boldsymbol{\beta}}_{***} - \hat{\boldsymbol{\beta}}_*) + \\
&\quad (\mathbf{Y} - X\hat{\boldsymbol{\beta}}_*)^T (\mathbf{Y} - X\hat{\boldsymbol{\beta}}_*) + \hat{\boldsymbol{\beta}}_*^T D_{\tilde{\boldsymbol{\tau}}}^{-1} \hat{\boldsymbol{\beta}}_* + 2\xi + f_2(\boldsymbol{\tau}, \tilde{\boldsymbol{\tau}}).
\end{aligned}$$

It follows from (S21) that

$$\begin{aligned}
& \int_{\mathbb{R}_+} \int_{\mathbb{R}_+} \int_{\mathbb{R}^p} \int_{\mathbb{R}^p} f(\tilde{\sigma}^2 \mid \tilde{\boldsymbol{\beta}}, \boldsymbol{\tau}, \mathbf{Y}) f(\tilde{\boldsymbol{\beta}} \mid \boldsymbol{\tau}, \sigma^2, \mathbf{Y}) f(\boldsymbol{\tau} \mid \boldsymbol{\beta}, \sigma^2, \mathbf{Y}) \\
& f(\boldsymbol{\beta} \mid \tilde{\boldsymbol{\tau}}, \sigma^2, \mathbf{Y}) f(\sigma^2 \mid \tilde{\boldsymbol{\beta}}, \tilde{\boldsymbol{\tau}}, \mathbf{Y}) f(\tilde{\boldsymbol{\tau}} \mid \tilde{\boldsymbol{\beta}}, \tilde{\sigma}^2, \mathbf{Y}) d\sigma^2 d\tilde{\sigma}^2 d\boldsymbol{\beta} d\tilde{\boldsymbol{\beta}} \\
& \geq f_3(\boldsymbol{\tau}, \tilde{\boldsymbol{\tau}}) \int_{\mathbb{R}^p} \left\{ \frac{1}{\left[f_4(\boldsymbol{\tau}, \tilde{\boldsymbol{\tau}}) + (\tilde{\boldsymbol{\beta}} - \hat{\boldsymbol{\beta}}_{***})^T (\mathbf{A}_\tau + \mathbf{A}_{\tilde{\boldsymbol{\tau}}}) (\tilde{\boldsymbol{\beta}} - \hat{\boldsymbol{\beta}}_{***}) \right]^{\frac{p}{2}}} d\tilde{\boldsymbol{\beta}} \right\} \\
& \geq \frac{f_3(\boldsymbol{\tau}, \tilde{\boldsymbol{\tau}})}{[f_4(\boldsymbol{\tau}, \tilde{\boldsymbol{\tau}})]^{\frac{p}{2}}} \int_{\mathbb{R}^p} \left\{ \frac{1}{\left[1 + (\tilde{\boldsymbol{\beta}} - \hat{\boldsymbol{\beta}}_{***})^T \frac{(\mathbf{A}_\tau + \mathbf{A}_{\tilde{\boldsymbol{\tau}}})}{f_4(\boldsymbol{\tau}, \tilde{\boldsymbol{\tau}})} (\tilde{\boldsymbol{\beta}} - \hat{\boldsymbol{\beta}}_{***}) \right]^{\frac{p}{2}}} d\tilde{\boldsymbol{\beta}} \right\} \\
& = \infty
\end{aligned}$$

for every $(\boldsymbol{\tau}, \tilde{\boldsymbol{\tau}}) \in \mathbb{R}_+^p \times \mathbb{R}_+^p$. The last integral is infinite based on the fact that the multivariate t -distribution with 1 degree of freedom has an infinite mean (see [Kotz and Nadarajah, 2004](#)). The first part of the result now follows from (S12).

We now focus on proving the second part of the result. In the current setting, to prove the trace class property for k , we need to show (see [Jorgens, 1982](#)) that

$$\iint_{\mathbb{R}^p \times \mathbb{R}_+} k((\boldsymbol{\beta}, \sigma^2), (\boldsymbol{\beta}, \sigma^2)) d\boldsymbol{\beta} d\sigma^2 < \infty. \quad (\text{S22})$$

It follows by (7) that

$$\begin{aligned} & \iint_{\mathbb{R}^p \times \mathbb{R}_+} k((\boldsymbol{\beta}, \sigma^2), (\boldsymbol{\beta}, \sigma^2)) d\boldsymbol{\beta} d\sigma^2 \\ &= \iiint_{\mathbb{R}^p \times \mathbb{R}_+^p \times \mathbb{R}_+} f(\boldsymbol{\tau} \mid \boldsymbol{\beta}, \sigma^2, \mathbf{Y}) f(\sigma^2 \mid \boldsymbol{\tau}, \mathbf{Y}) f(\boldsymbol{\beta} \mid \sigma^2, \boldsymbol{\tau}, \mathbf{Y}) d\boldsymbol{\beta} d\boldsymbol{\tau} d\sigma^2 \\ &= C_1 \iiint_{\mathbb{R}^p \times \mathbb{R}_+^p \times \mathbb{R}_+} \left(\prod_{j=1}^p \sqrt{\frac{\lambda^2}{2\pi}} (\tau_j)^{-\frac{1}{2}} \exp\left(-\frac{\beta_j^2 \left(1 - \tau_j \sqrt{\frac{\lambda^2 \sigma^2}{\beta_j^2}}\right)^2}{2\sigma^2 \tau_j}\right) \right) (\sigma^2)^{-\frac{n+2\alpha}{2}-1} \\ & \quad \exp\left(-\frac{1}{2\sigma^2} (\mathbf{Y}^T (I - X \mathbf{A}_\tau^{-1} X^T) \mathbf{Y} + 2\xi)\right) (\mathbf{Y}^T (I - X \mathbf{A}_\tau^{-1} X^T) \mathbf{Y} + 2\xi)^{\frac{n+2\alpha}{2}} (\sigma^2)^{-\frac{p}{2}} \\ & \quad \times |\mathbf{A}_\tau|^{-\frac{1}{2}} \times \exp\left(-\frac{(\boldsymbol{\beta} - \mathbf{A}_\tau^{-1} X^T \mathbf{Y})^T \mathbf{A}_\tau (\boldsymbol{\beta} - \mathbf{A}_\tau^{-1} X^T \mathbf{Y})}{2\sigma^2}\right) d\boldsymbol{\beta} d\boldsymbol{\tau} d\sigma^2 \\ &\stackrel{(a)}{\leq} C_2 \iiint_{\mathbb{R}^p \times \mathbb{R}_+^p \times \mathbb{R}_+} \frac{\exp\left(-\frac{\xi}{\sigma^2}\right) \exp\left(-\frac{1}{2\sigma^2} \sum_{j=1}^p \frac{\beta_j^2}{\tau_j} + \frac{\lambda}{\sigma} \sum_{j=1}^p |\beta_j| - \frac{\lambda^2}{2} \sum_{j=1}^p \tau_j\right)}{(\sigma^2)^{\frac{n+2\alpha}{2}+1} \prod_{j=1}^p (\tau_j)^{\frac{1}{2}}} \frac{|\mathbf{A}_\tau|^{-\frac{1}{2}}}{(\sigma^2)^{\frac{p}{2}}} \\ & \quad \times \exp\left(-\frac{1}{2\sigma^2} (\boldsymbol{\beta}^T \mathbf{A}_\tau \boldsymbol{\beta} - 2\boldsymbol{\beta}^T X^T \mathbf{Y} + \mathbf{Y}^T \mathbf{Y})\right) d\boldsymbol{\beta} d\boldsymbol{\tau} d\sigma^2, \end{aligned}$$

where

$$C_1 = \frac{1}{(2\pi)^{\frac{p}{2}} 2^{\frac{n+2\alpha}{2}} \Gamma\left(\frac{n+2\alpha}{2}\right)} \quad \text{and} \quad C_2 = (\mathbf{Y}^T \mathbf{Y} + 2\xi)^{\frac{n+2\alpha}{2}} \left(\frac{\lambda^2}{2\pi}\right)^{\frac{p}{2}} C_1.$$

Also, (a) follows from the fact that $\mathbf{Y}^T (I - X \mathbf{A}_\tau^{-1} X^T) \mathbf{Y} \leq \mathbf{Y}^T \mathbf{Y}$. For convenience, let

$$h(\sigma^2) = \exp\left(-\frac{\xi}{\sigma^2}\right) (\sigma^2)^{-\frac{n+2\alpha}{2}-1}.$$

It follows that

$$\begin{aligned}
& \iint_{\mathbb{R}^p \times \mathbb{R}_+} k((\boldsymbol{\beta}, \sigma^2), (\boldsymbol{\beta}, \sigma^2)) d\boldsymbol{\beta} d\sigma^2 \\
& \leq C_2 \iiint_{\mathbb{R}^p \times \mathbb{R}_+^p \times \mathbb{R}_+} h(\sigma^2) \frac{\exp\left(-\frac{1}{2\sigma^2} \sum_{j=1}^p \frac{\beta_j^2}{\tau_j} + \frac{\lambda}{\sigma} \sum_{j=1}^p |\beta_j| - \frac{\lambda^2}{2} \sum_{j=1}^p \tau_j\right) |\mathbf{A}_\tau|^{\frac{1}{2}}}{\prod_{j=1}^p (\tau_j)^{\frac{1}{2}} (\sigma^2)^{\frac{p}{2}}} \\
& \quad \times \exp\left(-\frac{1}{2\sigma^2} (\boldsymbol{\beta}^T \mathbf{A}_\tau \boldsymbol{\beta} - 2\boldsymbol{\beta}^T X^T \mathbf{Y} + \mathbf{Y}^T \mathbf{Y})\right) d\boldsymbol{\beta} d\tau d\sigma^2 \\
& = C_2 \iiint_{\mathbb{R}^p \times \mathbb{R}_+^p \times \mathbb{R}_+} \frac{h(\sigma^2)}{\prod_{j=1}^p (\tau_j)^{\frac{1}{2}}} \exp\left(-\frac{1}{2\sigma^2} \sum_{j=1}^p \frac{\beta_j^2}{\tau_j} + \frac{\lambda}{\sigma} \sum_{j=1}^p |\beta_j| - \frac{\lambda^2}{2} \sum_{j=1}^p \tau_j\right) \frac{|\mathbf{A}_\tau|^{\frac{1}{2}}}{(\sigma^2)^{\frac{p}{2}}} \\
& \quad \times \exp\left(-\frac{\boldsymbol{\beta}^T D_\tau^{-1} \boldsymbol{\beta}}{4\sigma^2}\right) \exp\left(-\frac{\boldsymbol{\beta}^T D_\tau^{-1} \boldsymbol{\beta}}{4\sigma^2}\right) \exp\left(-\frac{(\mathbf{Y} - X\boldsymbol{\beta})^T (\mathbf{Y} - X\boldsymbol{\beta})}{2\sigma^2}\right) d\boldsymbol{\beta} d\tau d\sigma^2 \\
& \leq C_2 \iiint_{\mathbb{R}^p \times \mathbb{R}_+^p \times \mathbb{R}_+} \frac{h(\sigma^2)}{\prod_{j=1}^p (\tau_j)^{\frac{1}{2}}} \exp\left(-\left(\frac{1}{2} + \frac{1}{4}\right) \frac{1}{\sigma^2} \sum_{j=1}^p \frac{\beta_j^2}{\tau_j} + \frac{\lambda}{\sigma} \sum_{j=1}^p |\beta_j| - \lambda^2 \left(\frac{1}{3} + \frac{1}{6}\right) \sum_{j=1}^p \tau_j\right) \\
& \quad \times \frac{|\mathbf{A}_\tau|^{\frac{1}{2}}}{(\sigma^2)^{\frac{p}{2}}} \exp\left(-\frac{\boldsymbol{\beta}^T D_\tau^{-1} \boldsymbol{\beta}}{4\sigma^2}\right) d\boldsymbol{\beta} d\tau d\sigma^2 \\
& = C_2 \iiint_{\mathbb{R}_+ \times \mathbb{R}_+^p \times \mathbb{R}^p} \frac{h(\sigma^2)}{\prod_{j=1}^p (\tau_j)^{\frac{1}{2}}} \exp\left(-\left(\frac{3}{4\sigma^2} \sum_{j=1}^p \frac{\beta_j^2}{\tau_j} - \frac{\lambda}{\sigma} \sum_{j=1}^p |\beta_j| + \frac{\lambda^2}{3} \sum_{j=1}^p \tau_j\right)\right) \frac{|\mathbf{A}_\tau|^{\frac{1}{2}}}{(\sigma^2)^{\frac{p}{2}}} \\
& \quad \times \exp\left(-\frac{\lambda^2}{6} \sum_{j=1}^p \tau_j\right) \exp\left(-\frac{\boldsymbol{\beta}^T D_\tau^{-1} \boldsymbol{\beta}}{4\sigma^2}\right) d\boldsymbol{\beta} d\tau d\sigma^2.
\end{aligned}$$

Note that

$$\exp\left(-\left(\frac{3}{4\sigma^2} \sum_{j=1}^p \frac{\beta_j^2}{\tau_j} - \frac{\lambda}{\sigma} \sum_{j=1}^p |\beta_j| + \frac{\lambda^2}{3} \sum_{j=1}^p \tau_j\right)\right) = \prod_{j=1}^p \exp\left(-\left(\frac{\sqrt{3\beta_j^2}}{2\sigma\sqrt{\tau_j}} - \frac{\sqrt{\lambda^2\tau_j}}{\sqrt{3}}\right)^2\right) \leq 1,$$

and

$$\int_{\mathbb{R}^p} \exp\left(-\frac{\boldsymbol{\beta}^T D_\tau^{-1} \boldsymbol{\beta}}{4\sigma^2}\right) d\boldsymbol{\beta} = \frac{(4\pi)^{p/2} (\sigma^2)^{p/2}}{|D_\tau^{-1}|^{1/2}}.$$

It follows that

$$\begin{aligned}
& \iint_{\mathbb{R}^p \times \mathbb{R}_+} k((\boldsymbol{\beta}, \sigma^2), (\boldsymbol{\beta}, \sigma^2)) d\boldsymbol{\beta} d\sigma^2 \\
& \leq (4\pi)^{\frac{p}{2}} C_2 \iint_{\mathbb{R}_+ \times \mathbb{R}_+^p} \frac{h(\sigma^2)}{\prod_{j=1}^p (\tau_j)^{\frac{1}{2}}} \exp\left(-\frac{\lambda^2}{6} \sum_{j=1}^p \tau_j\right) \frac{|\mathbf{A}_{\boldsymbol{\tau}}|^{\frac{1}{2}}}{(\sigma^2)^{\frac{p}{2}}} \frac{(\sigma^2)^{\frac{p}{2}}}{|D_{\boldsymbol{\tau}}^{-1}|^{\frac{1}{2}}} d\boldsymbol{\tau} d\sigma^2 \\
& \leq (4\pi)^{\frac{p}{2}} C_2 \left(\int_{\mathbb{R}_+} h(\sigma^2) d\sigma^2 \right) \left(\int_{\mathbb{R}_+^p} \frac{|\mathbf{A}_{\boldsymbol{\tau}}|^{\frac{1}{2}}}{|D_{\boldsymbol{\tau}}^{-1}|^{\frac{1}{2}}} \frac{1}{\prod_{j=1}^p (\tau_j)^{\frac{1}{2}}} \exp\left(-\frac{\lambda^2}{6} \sum_{j=1}^p \tau_j\right) d\boldsymbol{\tau} \right) \\
& = (4\pi)^{\frac{p}{2}} C_2 \Gamma\left(\frac{n+2\alpha}{2}\right) \xi^{-\frac{n+2\alpha}{2}} \int_{\mathbb{R}_+^p} |\mathbf{A}_{\boldsymbol{\tau}}|^{\frac{1}{2}} \exp\left(-\frac{\lambda^2}{6} \sum_{j=1}^p \tau_j\right) d\boldsymbol{\tau}
\end{aligned}$$

Hence, to prove the required result, it is enough to show that

$$\int_{\mathbb{R}_+^p} |\mathbf{A}_{\boldsymbol{\tau}}|^{\frac{1}{2}} \exp\left(-\frac{\lambda^2}{6} \sum_{j=1}^p \tau_j\right) d\boldsymbol{\tau} < \infty. \quad (\text{S23})$$

Let c^2 denote the maximum eigenvalue of $X^T X$. Then, by the results of [Fiedler \(1971\)](#), it follows that

$$\begin{aligned}
|\mathbf{A}_{\boldsymbol{\tau}}|^{1/2} & \leq \prod_{j=1}^p \sqrt{\left(c^2 + \frac{1}{\tau_j}\right)} \leq \prod_{j=1}^p \left(\sqrt{c^2} + \frac{1}{\sqrt{\tau_j}}\right) \\
& = c^p + \left(\frac{1}{\sqrt{\tau_1}} + \frac{1}{\sqrt{\tau_2}} + \cdots + \frac{1}{\sqrt{\tau_p}}\right) c^{p-1} + \left(\frac{1}{\sqrt{\tau_1 \tau_2}} + \cdots + \frac{1}{\tau_i \tau_j} + \cdots\right) c^{p-2} + \\
& \quad \cdots + \frac{1}{\sqrt{\tau_1 \tau_2 \cdots \tau_p}}.
\end{aligned} \quad (\text{S24})$$

It follows from [\(S24\)](#) that

$$\begin{aligned}
& \int_{\mathbb{R}_+^p} |\mathbf{A}_{\boldsymbol{\tau}}|^{\frac{1}{2}} \exp\left(-\frac{\lambda^2}{6} \sum_{j=1}^p \tau_j\right) d\boldsymbol{\tau} \\
& \leq c^p \int_{\mathbb{R}_+^p} \exp\left(-\frac{\lambda^2}{6} \sum_{j=1}^p \tau_j\right) d\boldsymbol{\tau} + c^{p-1} \int_{\mathbb{R}_+^p} \left(\frac{1}{\sqrt{\tau_1}} + \frac{1}{\sqrt{\tau_2}} + \cdots + \frac{1}{\sqrt{\tau_p}}\right) \exp\left(-\frac{\lambda^2}{6} \sum_{j=1}^p \tau_j\right) d\boldsymbol{\tau} + \\
& \quad c^{p-2} \int_{\mathbb{R}_+^p} \left(\frac{1}{\sqrt{\tau_1 \tau_2}} + \cdots + \frac{1}{\sqrt{\tau_i \tau_j}} + \cdots\right) \exp\left(-\frac{\lambda^2}{6} \sum_{j=1}^p \tau_j\right) d\boldsymbol{\tau} + \\
& \quad \cdots + \int_{\mathbb{R}_+^p} \frac{1}{\sqrt{\tau_1 \tau_2 \cdots \tau_p}} \exp\left(-\frac{\lambda^2}{6} \sum_{j=1}^p \tau_j\right) d\boldsymbol{\tau}.
\end{aligned} \quad (\text{S25})$$

Now, note that for any $m \in \{1, 2, \dots, p\}$,

$$\begin{aligned} & \int_{\mathbb{R}_+^p} \frac{1}{\sqrt{\tau_{i_1}} \sqrt{\tau_{i_2}} \cdots \sqrt{\tau_{i_m}}} \exp\left(-\frac{\lambda^2}{6} \sum_{j=1}^p \tau_j\right) d\tau \\ &= \left(\frac{6}{\lambda^2}\right)^{p-m} \left(\int_{\mathbb{R}_+} \frac{1}{\sqrt{\tau_{i_1}}} e^{-\frac{\lambda^2}{6} \tau_{i_1}} d\tau_{i_1}\right) \times \cdots \times \left(\int_{\mathbb{R}_+} \frac{1}{\sqrt{\tau_{i_m}}} e^{-\frac{\lambda^2}{6} \tau_{i_m}} d\tau_{i_m}\right) < \infty. \quad (\text{S26}) \end{aligned}$$

The result now follows by (S23), (S25) and (S26). \square

S2 Additional Numerical Results

Figure S4 is similar to the left-hand side of Figure 2 under settings of high multicollinearity (left), low sparsity (center), and both high multicollinearity and low sparsity (right). (See the following section for details.) It is clear that the behavior seen in Figure 1 is also seen in other settings of multicollinearity and sparsity.

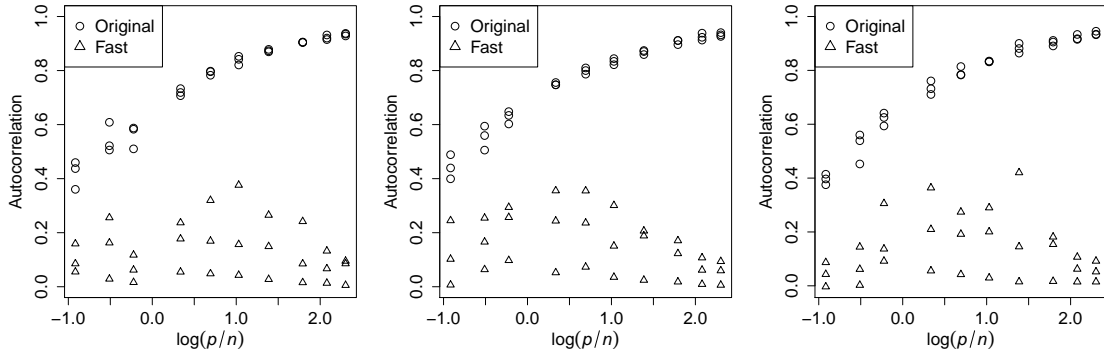


Figure S4: Autocorrelation of the σ_k^2 chain versus p/n for various values of n for the original and two-step Bayesian lasso Gibbs samplers in settings of high multicollinearity (left), low sparsity (center), and both high multicollinearity and low sparsity (right). See the following section for details of the generation of the numerical quantities used in the execution of these chains.

S3 Details of Numerical Results

Each plotted point in Figures 1 and 2 represents the average lag-one autocorrelation over 10 Gibbs sampling runs of 10,000 iterations each (after discarding an initial “burn-in” period of 1,000 iterations). For each of the 10 runs at each n and p setting, the np elements of the $n \times p$ covariate matrix \mathbf{X} were first drawn as $N(0, 1)$ random variables with all pairwise correlations equal to $1/5$. The columns of \mathbf{X} were then standardized to have mean zero and

squared Euclidean norm n . Also, for each run, the $n \times 1$ response vector \mathbf{Y} was generated as $\mathbf{Y} = \mathbf{X}\boldsymbol{\beta}_\star + \boldsymbol{\varepsilon}$, where $\boldsymbol{\beta}_\star$ is a $p \times 1$ vector with its first $\lceil p/5 \rceil$ elements drawn as independent t_2 random variables and its remaining $p - \lceil p/5 \rceil$ elements set to zero, and where $\boldsymbol{\varepsilon}$ is an $n \times 1$ vector of independent t_4 random variables. The initial values were set as $\boldsymbol{\beta}_0 = \mathbf{1}_p$ and $\sigma_0^2 = 1$. The regularization parameter λ was set to $\lambda = 1$. In Figure 1, for each n , the values of p were $2n$, $4n$, $6n$, $8n$, and $10n$. The left side of Figure 2 includes the same results as in Figure 1 but also includes p equal to $2n/5$, $3n/5$, $4n/5$, $7n/5$, and $14n/5$. The DAF surface plots in the center and right side of Figure 2 used each combination of $n, p \in \{5, 15, 25, 35, 45\}$.

For the examples in Section 5, the starting points of all chains were set as $\boldsymbol{\beta}_0 = \mathbf{1}_p$ and $\sigma_0^2 = 1$. For the crime data in Subsection 5.3, the $p = 1325$ covariates were the 50 first-order terms, 50 quadratic terms, and 1225 multiplicative interaction terms involving 50 first-order covariates, which themselves were chosen as follows. First, all potential covariates with missing data were excluded, which left 99 potential covariates. Next, any remaining potential covariates for which over half of the values were equal to any single value were excluded, which left 94 potential covariates. From the remaining potential covariates, we selected the 50 with the largest absolute correlation with the response vector. These 50 chosen covariates were then standardized to have mean zero before the second-order terms were computed. From the 1994 total observations, $n = 10$ were chosen at random. The final columns of the design matrix (now with $n = 10$ rows) were then standardized again to have mean zero and squared Euclidean norm n .

For the numerical results of the spike-and-slab sampler in Subsection 5.1.2, all settings were identical to those used for the corresponding results for the Bayesian lasso, with the obvious exception of the hyperparameters in the prior. The hyperparameters of the spike-and-slab prior were set as $w_j = 1/2$ and $\kappa_j = 100$ for each $j \in \{1, \dots, p\}$. For the gene expression data, we set $\zeta_j = 0.00002$ for each $j \in \{1, \dots, p\}$. For the simulated data, we set $\zeta_j = 0.01$ for each $j \in \{1, \dots, p\}$.

The plots in Figure S4 were constructed similarly to the left-hand side of Figure 2, but with the following additional modifications. For the left-hand side and the right-hand side (but not the center), the pairwise correlation between each element of the design matrix was $4/5$ (rather than $1/5$). For the center and right-hand side (but not the left-hand side), the number of nonzero coefficients for the generation of the response vector was taken to be $\lceil 4p/5 \rceil$ (rather than $\lceil p/5 \rceil$).

The R function `set.seed` was used to initialize the random number generation. Different seeds were used for each data set and each collection of simulations to facilitate reproducibility of individual figures and results. The seeds themselves were taken as consecutive three-digit blocks of the decimal expansion of π (i.e., 141, 592, 653, etc.) to make absolutely clear that

they were not manipulated to gain any advantage for the proposed methodology. The reader can of course verify directly that the results are qualitatively similar for other seeds.

S4 R Code

The R code for generating the numerical results of Sections 4, 5, and S2 is provided in its entirety in an accompanying file. This code incorporates functions or data from the R packages `coda` (Plummer et al., 2006), `flare` (Li et al., 2014), `lars` (Hastie and Efron, 2013), `ppls` (Kramer et al., 2008), and `statmod` (Smyth et al., 2014). We also reproduce below the portion of the R code that executes the original and two-step Bayesian lasso algorithms themselves.

```
# Slightly modified version of rinvgauss function from statmod package
rinvgauss. <- function(n,mean=1,shape=NULL,dispersion=1){
  if(!is.null(shape)){dispersion <- 1/shape}
  mu <- rep_len(mean,n)
  phi <- rep_len(dispersion,n)
  r <- rep_len(0,n)
  i <- (mu>0 & phi>0)
  if(!all(i)){
    r[!i] <- NA
    n <- sum(i)
  }
  phi[i] <- phi[i]*mu[i]
  Y <- rchisq(n,df=1)
  X1 <- 1+phi[i]/2*(Y-sqrt(4*Y/phi[i]+Y^2))
  # Note: The line above should yield all X1>0, but it occasionally doesn't due to
  # numerical precision issues. The line below detects this and recomputes
  # the relevant elements of X1 using a 2nd-order Taylor expansion of the
  # sqrt function, which is a good approximation whenever the problem occurs.
  if(any(X1<=0)){X1[X1<=0] <- (1/(Y*phi[i]))[X1<=0]}
  firstroot <- as.logical(rbinom(n,size=1L,prob=1/(1+X1)))
  r[i][firstroot] <- X1[firstroot]
  r[i][!firstroot] <- 1/X1[!firstroot]
  mu*r
}

# Draw from inverse-Gaussian distribution while avoiding potential numerical problems
rinvgaussian <- function(n,m,l){
  m. <- m/sqrt(m*l)
  l. <- l/sqrt(m*l)
  sqrt(m*l)*rinvgauss.(n,m.,l.)
}
```

```

# Gibbs iteration functions for both Bayesian lassos
# Note: The versions have separate functions, as opposed to being different
#       options of the same function, since the latter would require checking any such
#       options every time the function is called, i.e., in every MCMC iteration.
# Note: The values of XTY, n, and p can obviously be calculated from X and Y, but they
#       are included as inputs to avoid recalculating them every time the function is
#       called, i.e., in every MCMC iteration.
iter.bl.original <- function(beta,sigma2,X,Y,XTY,n,p,lambda){
  d.tau.inv <- rinvgaussian(p,sqrt(lambda^2*sigma2/beta^2),lambda^2)
  A.chol <- chol(t(X)%*%X+diag(d.tau.inv))
  beta.tilde <- backsolve(A.chol,backsolve(t(A.chol),XTY,upper.tri=F))
  Z <- rnorm(p)
  beta.new <- beta.tilde+sqrt(sigma2)*backsolve(A.chol,Z)
  sigma2.new <- (sum((Y-drop(X)%*%beta.new))^2)+
    sum(beta.new^2*d.tau.inv))/rchisq(1,n+p-1)
  return(list(beta=beta.new,sigma2=sigma2.new))
}

iter.bl.fast <- function(beta,sigma2,X,Y,XTY,n,p,lambda){
  d.tau.inv <- rinvgaussian(p,sqrt(lambda^2*sigma2/beta^2),lambda^2)
  A.chol <- chol(t(X)%*%X+diag(d.tau.inv))
  beta.tilde <- backsolve(A.chol,backsolve(t(A.chol),XTY,upper.tri=F))
  sigma2.new <- (sum(Y^2)-sum(XTY*beta.tilde))/rchisq(1,n-1)
  Z <- rnorm(p)
  beta.new <- beta.tilde+sqrt(sigma2.new)*backsolve(A.chol,Z)
  return(list(beta=beta.new,sigma2=sigma2.new))
}

# Run original and two-step Bayesian lassos
run.bl <- function(X,Y,lambda,K,M,outfile.stem,fast=F,keep.beta=T,write.each=F){
  XTY <- drop(t(X)%*%Y)
  n <- dim(X)[1]
  p <- dim(X)[2]
  iter.bl <- get(paste("iter.bl.",ifelse(fast,"fast","original"),sep=""))
  chindigits <- max(1,ceiling(log(M,10))) # digits needed for chain label strings
  for(chain in 0:(M-1)){
    beta <- rep(1,p)
    sigma2 <- 1
    chaintext <- substring(format(chain/(10^chindigits),nsmall=chindigits),3)
    outfile.beta <- paste(outfile.stem,"-",chaintext,"-b.txt",sep="")
    outfile.sigma2 <- paste(outfile.stem,"-",chaintext,"-s.txt",sep="")
    if(write.each){
      for(k in 1:K){

```

```

iter.result <- iter.bl(beta,sigma2,X,Y,XTY,n,p,lambda)
beta <- iter.result$beta
sigma2 <- iter.result$sigma2
if(keep.beta){
beta.row <- matrix(beta,nrow=1)
write.table(beta.row,outfile.beta,append=T,row.names=F,col.names=F)
}
write.table(sigma2,outfile.sigma2,append=T,row.names=F,col.names=F)
}
}else{
beta.chain <- matrix(NA,nrow=K,ncol=p)
sigma2.chain <- rep(NA,K)
for(k in 1:K){
iter.result <- iter.bl(beta,sigma2,X,Y,XTY,n,p,lambda)
beta <- iter.result$beta
sigma2 <- iter.result$sigma2
beta.chain[k,] <- beta
sigma2.chain[k] <- sigma2
}
if(keep.beta){
write.table(beta.chain,outfile.beta,row.names=F,col.names=F)
}
write.table(sigma2.chain,outfile.sigma2,row.names=F,col.names=F)
}
typetext <- ifelse(fast,"Fast","Orig")
print(paste(typetext,"chain",chain+1,"of",M,"complete at",date()))
flush.console()
}
}

```

References

- ARMAGAN, A., B., D. D. D. and LEE, J. (2013a). Generalized double pareto shrinkage. *Statistica Sinica*, **23** 119–143.
- ARMAGAN, A., DUNSON, D. B. and LEE, J. (2013b). Generalized double pareto shrinkage. *Statistica Sinica*, **23**.
- BHATTACHARYA, A., PATI, D., PILLAI, N. S. and DUNSON, D. B. (2015). Dirichlet-laplace priors for optimal shrinkage. *Journal of the American Statistical Association*, *in press*.

- BROWN, P. J., FEARN, T. and VANNUCCI, M. (2001). Bayesian wavelet regression on curves with applications to a spectroscopic calibration problem. *Journal of the American Statistical Association*, **96** 398–408.
- CARVALHO, C., POLSON, N. and SCOTT, J. (2010). The horseshoe estimator for sparse signals. *Biometrika*, **97** 465–480.
- DE LOS CAMPOS, G., NAYA, H., GIANOLA, D., CROSSA, J., LEGARRA, A., MANFREDI, E., WEIGEL, K. and COTES, J. M. (2009). Predicting quantitative traits with regression models for dense molecular markers and pedigree. *Genetics*, **182** 375–385.
- DEMIGUEL, V., GARLAPPI, L., NOGALES, F. J. and UPPAL, R. (2009). A generalized approach to portfolio optimization: improving performance by constraining portfolio norms. *Management Science*, **55** 798–812.
- FIEDLER, M. (1971). Bounds for the determinant of the sum of hermitian matrices. *Proceedings of the American Mathematical Society*, **30** 27–31.
- GELMAN, A., CARLIN, J. B., STERN, H. S., DUNSON, D. B., VEHTARI, A. and RUBIN, D. B. (2013). *Bayesian Data Analysis*. Chapman and Hall/CRC.
- GEORGE, E. I. and MCCULLOCH, R. E. (1993). Variable selection via Gibbs sampling. *Journal of the American Statistical Association*, **88** 881–889.
- GRIFFIN, J. and BROWN, P. (2010). Inference with normal-gamma prior distributions in regression problems. *Bayesian Analysis*, **5** 171–188.
- GU, X., YIN, G. and LEE, J. J. (2013). Bayesian two-step lasso strategy for biomarker selection in personalized medicine development for time-to-event endpoints. *Contemporary Clinical Trials*, **36** 642–650.
- HANS, C. (2009). Bayesian lasso regression. *Biometrika*, **96** 835–845.
- HASTIE, T. and EFRON, B. (2013). lars: Least angle regression, lasso and forward stagewise. *R package version 1.2*, URL <http://CRAN.R-project.org/package=lars>.
- HOBERT, J. P. and MARCHEV, D. (2008). A theoretical comparison of the data augmentation, marginal augmentation and px-da algorithms. *The Annals of Statistics*, **36**.
- JACQUEMIN, S. J. and DOLL, J. C. (2014). Body size and geographic range do not explain long term variation in fish populations: a bayesian phylogenetic approach to testing assembly processes in stream fish assemblages. *PLoS ONE*, **9** 1–7.

- JONES, G. L. and HOBERT, J. P. (2001). Honest exploration of intractable probability distributions via Markov chain Monte Carlo. *Statistical Science*, **16** 312–334.
- JORGENS, K. (1982). *Linear Integral Operators*. Pitman Books.
- KHARE, K. and HOBERT, J. P. (2011). A spectral analytic comparison of trace-class data augmentation algorithms and their sandwich variants. *The Annals of Statistics*, **39**.
- KHARE, K. and HOBERT, J. P. (2013). Geometric ergodicity of the Bayesian lasso. *Electronic Journal of Statistics*, **7** 2150–2163.
- KOTZ, S. and NADARAJAH, S. (2004). *Multivariate t Distributions and Their Applications*. Cambridge University Press.
- KRAMER, N., BOULESTEIX, A.-L. and TUTZ, G. (2008). Penalized partial least squares with applications to b-spline transformations and functional data. *Chemometrics and Intelligent Laboratory Systems*, **94** 60–69.
- KYUNG, M., GILL, J., GHOSH, M. and CASELLA, G. (2010). Penalized regression, standard errors, and Bayesian lassos. *Bayesian Analysis*, **5** 369–412.
- LI, Q. and LIN, N. (2010). The Bayesian elastic net. *Bayesian Analysis*, **5** 151–170.
- LI, X., ZHAO, T., WANG, L., YUAN, X. and LIU, H. (2014). flare: Family of lasso regression. r package version 1.5.0. URL <http://CRAN.R-project.org/package=flare>.
- LICHMAN, M. (2013). Uci machine learning repository. URL <http://archive/ics.uci.edu/ml>.
- LIU, J. S., WONG, W. H. and KONG, A. (1994). Covariance structure of the Gibbs sampler with applications to the comparisons of estimators and augmentation schemes. *Biometrika*, **81** 27–40.
- LIU, J. S. and WU, Y. N. (1999). Parameter expansion for data augmentation. *J. Amer. Statist. Assoc.*, **94** 1264–1274.
- MENG, X. L. and VAN DYK, D. A. (1999). Seeking efficient data augmentation schemes via conditional and marginal augmentation. *Biometrika*, **86** 301–320.
- MISHCHENKO, Y. and PANINSKI, L. (2012). A bayesian compressed-sensing approach for reconstructing neural connectivity from subsampled anatomical data. *Journal of Computational Neuroscience*, **33** 371–388.

- MITCHELL, T. J. and BEAUCHAMP, J. J. (1988). Bayesian variable selection in linear regression (with discussion). *Journal of the American Statistical Association*, **83** 1023–1036.
- OSBORNE, B. G., FEARN, T., MILLER, A. R. and DOUGLAS, S. (1984). Application of near infrared reflectance spectroscopy to the compositional analysis of biscuits and biscuit doughs. *Journal of the Science of Food and Agriculture*, **35** 99–105.
- PAL, S. and KHARE, K. (2014). Geometric ergodicity for bayesian shrinkage models. *Electronic Journal of Statistics*, **8** 604–645.
- PARK, T. and CASELLA, G. (2008). The Bayesian lasso. *Journal of the American Statistical Association*, **103** 681–686.
- PLUMMER, M., BEST, N., COWLES, K. and VINES, K. (2006). Coda: Convergence diagnosis and output analysis for mcmc. *R News*, **6** 7–11.
- POLSON, N. and SCOTT, J. (2010). Shrink globally, act locally: Sparse bayesian regularization and prediction. *Bayesian Statistics 9 (J.M. Bernardo, M.J. Bayarri, J.O. Berger, A.P. Dawid, D. Heckerman, A.F.M. Smith and M. West, eds.)*, Oxford University Press, New York 501–538.
- POLSON, N. G., SCOTT, J. G. and WINDLE, J. (2013). Bayesian inference for logistic models using Polya-Gamma latent variables. *Journal of the American Statistical Association*, **108** 1339–1349.
- PONG-WONG, R. (2014). Estimation of genomic breeding values using the horseshoe prior. *BMC Proc.*, **8** Suppl 5.
- PONG-WONG, R. and WOOLLIAMS, J. (2014). Bayes u: A genomic prediction method based on the horseshoe prior. 10, World Congress of Genetics Applied to Livestock Production, Vancouver, Canada.
- RAJARATNAM, B. and SPARKS, D. (2015). MCMC-based inference in the era of big data: A fundamental analysis of the convergence complexity of high-dimensional chains. <http://arxiv.org/abs/1508.00947>. Tech. rep., Stanford University.
- REDMOND, M. and BAVEJA, A. (2002). A data-driven software tool for enabling cooperative information sharing among police departments. *European Journal of Operations Research*, **141** 660–678.
- ROSENTHAL, J. S. (1995). Minorization conditions and convergence rates for Markov chain Monte Carlo. *Journal of the American Statistical Association*, **90** 558–566.

- SCHEETZ, T. E., KIM, K.-Y. A., SWIDERSKI, R. E., PHILIP, A. R., BRAUN, T. A., KNUDTSON, K. L., DORRANCE, A. M., DiBONA, G. F., HUANG, J., CASAVANT, T. L., SHEFFIELD, V. C. and STONE, E. M. (2006). Regulation of gene expression in the mammalian eye and its relevance to eye disease. *Proceedings of the National Academy of Sciences of the United States of America*, **103** 14429–14434.
- SMYTH, G., HU, Y., DUNN, P., Phipson, B. and CHEN, Y. (2014). statmod: Statistical modeling. *R package version 1.4.20*, URL <http://CRAN.R-project.org/package=statmod>.
- TEAM, R. C. (2014). R: A language and environment for statistical computing. *R Foundation for Statistical Computing, Vienna, Austria*. URL <http://www.R-project.org/>.
- TIBSHIRANI, R. (1996). Regression shrinkage and selection via the lasso. *Journal of the Royal Statistical Society, Series B*, **58** 267–288.
- XING, Z., ZHOU, M., CASTRODAD, A., SAPIRO, G. and CARIN, L. (2012). Dictionary learning for noisy and incomplete hyperspectral images. *SIAM Journal of Imaging Sciences*, **5** 33–56.
- YI, N. and XU, S. (2008). Bayesian lasso for quantitative trait loci mapping. *Genetics*, **179** 1045–1055.